2003

Modelling stored grain microclimates with dual-region heat transfer models

Alexsandar Antic
University of Wollongong

Modelling Stored Grain Microclimates with Dual-Region Heat Transfer Models

A thesis submitted in fulfillment of the

requirements for the award of the degree of

Doctor of Philosophy

from

University of Wollongong

by

Alexsandar Antic

B.Math.(Hons), B.Comp.Sc., UOW

School of Mathematics and Applied Statistics

2003

This thesis is submitted to the University of Wollongong, and has not been submitted for a degree to any other University or Institution.

Alexsandar Antic

December, 2002

Dedicated to my grandfather

As far as the laws of mathematics refer to reality,
they are not certain;
and as far as they are certain,
they do not refer to reality.

Albert Einstein

Acknowledgements

First of all, I would like to thank my supervisor Professor Jim Hill and my co-supervisor Mr James Darby for their moral and academic support throughout the duration of the PhD. I would also like to thank Associate Professor Tim Marchant for his time and detailed feedback and Dr Grant Cox for his help.

I would like to acknowledge the Bulk Handling Companies of Australia for provision of a postgraduate scholarship.

A special thanks to all the PhD students and staff at the School of Mathematics and Applied Statistics, University of Wollongong, and to all the staff at the Stored Grain Research Laboratory, CSIRO Entomology, which this work has been done in collaboration with, who made the whole experience so memorable.

A very special thanks to Katrina Mather who always managed to bring a smile to my face. May the following words bring a smile to yours:

Part of the secret of success in life is to eat what you like

and let the food fight it out inside.

- Mark Twain

Also, a very special thanks to Matthew Lee, a great friend and thought-provoking room-mate, may you ponder over these words:

A pessimist sees the difficulty in every opportunity;

an optimist sees the opportunity in every difficulty.

- Sir Winston Churchill

Finally, to my loving and supportive family, *mnogo hvala vama za sve.*

Abstract

Australia's reputation is well established in the international marketplace as a producer of high-quality grain. We remain competitive by exporting grain in accordance with a 'nil tolerance' for live insects. Protecting the grain while in storage means maintaining such a reputation is difficult and costly as one must deal with such factors as varying climatic conditions, particularly temperature, which can have an adverse affect on grain quality and insect infestation. An understanding of the flow of heat in grain store structures is very important from many industrial perspectives, and the heat transfer within the *peripheral layer* is of particular importance. To analyse the heat-transfer within such regions, we develop two mathematical models known as the *double-diffusivity heat transfer model* and the *two-stage heat transfer model*, and since the grain bulk is composed of predominantly air and grain, we make this distinction in our models. Semi-analytical and numerical approximations are obtained for both models from which the overall variation in temperature close to the grain store wall may be predicted. Very good agreement is obtained between the two solutions for both models. Good agreement is also obtained between the double-diffusivity heat transfer and two-stage heat transfer models.

Currently, there is an ongoing reduction in the number of chemicals permitted for pest control, as insects have developed resistance to some chemicals and others are currently being phased out due to safety and environmental reasons. As a result, the grain storage industry is moving towards physical methods as opposed to chemical methods, as a safer and potentially better alternative. One well studied area is

known as *thermal disinfestation*, with one of the potentially best forms being *heat disinfestation via microwave radiation.* The mathematical modelling of microwave heating processes in general requires the solution of a complex system of equations, which can be very difficult to obtain. In this work we illustrate the possibility of reducing the problem to one which involves extending the double-diffusivity heat transfer model which we develop to include a non-linear body heating source term to account for the heating due to microwave radiation. This model is known as the *double-diffusivity heat transfer model incorporating microwave heating.* Very good agreement is found between the semi-analytical and numerical approximations obtained.

These models are of practical importance because at present there is no experimental data available due to the difficulty involved in measuring air and grain temperatures separately, particularly within the peripheral layer. The proposed modelling by either linear or relatively simple non-linear models, allows semi-analytical approximations to be obtained in order to provide important insight into the potential difference that exists between the air and grain temperatures, in particular, for small time and spatial scales. We comment that this work forms the foundations for subsequent work to what is a very complex practical problem, which we believe will ultimately lead to a better understanding of the microclimate within the peripheral layer of a grain bulk.

Contents

List of Figures

Nomenclature

T_a is the temperature of the air

T_g is the temperature of the grain

K_a is the thermal diffusivity of the air

K_g is the thermal diffusivity of the grain

k_a is the *effective* heat transfer coefficient from air to grain or grain to air

κ_a is the thermal conductivity of the air

κ_g is the thermal conductivity of the grain

ρ_a is the density of the air

ρ_g is the density of the grain

c_a is the specific heat of the air at constant pressure

c_g is the specific heat of the grain at constant pressure

T_{a0} is the initial temperature of the air

T_{g0} is the initial temperature of the grain

T_0 is the initial temperature of the air and grain

T_b is the boundary temperature

Q is the body heating source term due to microwave radiation

r is the spatial coordinate system in the grain kernel

a is the radius of the grain kernel

Φ_a is the fraction of grain bulk volume occupied by air

P_f is the fluid pressure in the fissure system at position x at time t

P_b is the pressure change in the block at position y at time t located in the neighbourhood of position x

Φ_f is the porosity of the fissure system

Φ_b is the porosity of the blocks

μ is the dynamic viscosity of the fluid

c is the compressibility of the fluid at constant pressure

K_f is the permeability of the fissure system

K_b is the permeability of the blocks

V_x is the volume of block in the neighbourhood of position x

S_x is the surface of the block in the neighbourhood of position x

$\mathbf{E}$ is the electric field

$\mathbf{D}$ is the electric field displacement vector

$\mathbf{H}$ is the magnetic field

$\mathbf{B}$ is the magnetic flux density

p_f is the free charge density

$\mathbf{j_f}$ is the free current density

ϵ is the electric permittivity

ϵ' is the dielectric constant

ϵ'' is the loss factor

μ is the magnetic permeability

ω is the microwave frequency

σ is the electrical conductivity

E_o is the incident electric field amplitude

α is the decay constant of the electric field

Chapter 1

Introduction

1.1 Industrial Motivation

The stored product industry worldwide is undergoing continual and considerable change, and in Australia, the pace of change is very rapid. The motivation behind this is two-fold. First of all, there is the general issue of food safety, with grain buyers increasing their demand for high quality, pest and chemical free grain, which has resulted in stored grain being increasingly regarded as a stored food, not a raw material. The other issue is the on-going problem of the development of resistance by insect pests to most chemical treatments.

Australia's reputation is well established in the international marketplace for supplying grain which meets its customers strict requirements of being clean, high quality, and most important of all, insect-free. As a result of this, its product commands premium prices in the marketplace. To remain competitive, Australia exports a product in accordance with a 'nil tolerance' for live insects. As losses

from insects are relatively small, it is the presence of insects which is the critical factor [18].

Protecting the grain while in storage means maintaining such a reputation is difficult and costly. It is at this time that two main problems are encountered. Firstly, varying climatic conditions can have an adverse affect on grain quality and insect infestation, which is the second problem. To deal with these issues the grain industry has become heavily reliant on chemicals to preserve grain and control insect pests.

Winter crops make up most of the grain grown in Australia. They are harvested during summer and then stored. The grain is typically taken into storage warm (>25°C) and dry (<12% moisture content). Winter crops include wheat, barley, oats, lupins, field peas, mung beans, chickpeas and canola. Summer crops include rice, sorghum and maize, and are harvested at Easter. In general, it is the winter cereals that incur significant insect presence due to their warmer temperatures [17].

In recent years, psocids (psocoptera) have proved to be a very problematic pest for the Australian grain industry, and appear to be on the increase in storage systems around the country [52]. The most common psocids found infesting grain bulks are a wingless species of the genus (*Liposcelis* spp.) [53]. They are becoming serious structural pests which can exist for long periods without food, and as a result of their small size, can be extremely invasive. With increasing frequency, they have been found in huge numbers within grain bulks. Such infestations are increasingly a source of concern for an industry which strives to deliver insect-free grain [52]. They damage grain by feeding on it, and huge numbers with densities of several

thousand per kilogram have been recorded [53]. Such large numbers of psocids can cause blockages of contaminated grain at out-loading, as illustrated in Figure 1.1.

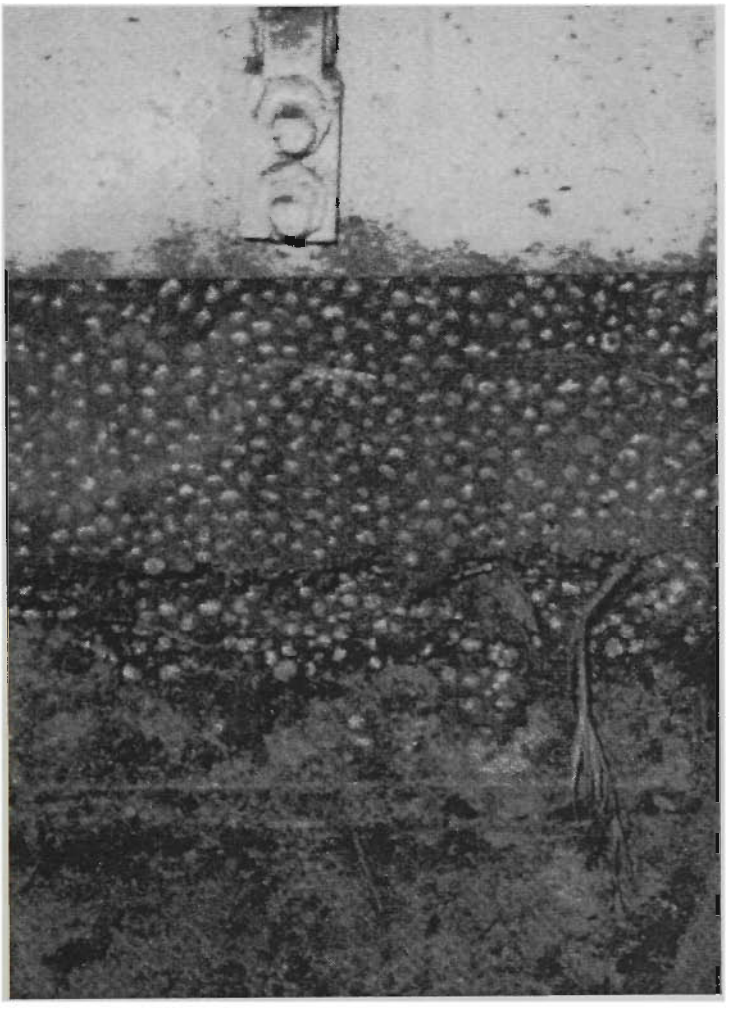

Figure 1.1: A silo exit chute blocked with psocids (dark) and grain (white).

One reason why these particular insects are a major problem is due to their ability to move rapidly in and out of infested grain bulks, apparently in response to climatic and environmental conditions, particularly temperature, rather than to the presence of a fumigant [52]. A fumigant is defined as a chemical that, at a required temperature and pressure, can exist in the gaseous state in sufficient concentrations to be lethal to a given pest organism [57]. This movement makes it difficult to control their populations by current pest control methods, such as chem-

ical fumigation, as their movement means that a number of them do not remain long enough within a fumigated grain bulk to absorb a lethal dosage of the fumigant, thus possibly surviving, and re-populating the grain bulk. Psocids exhibit the following characteristics:

- they are small and soft-bodied, with some 4000 species known worldwide,
- they are flattened and almost translucent in appearance, with long hair-like antennae, and are typically wingless, as seen in Figure 1.2,
- their typical dimensions measure 1mm in length, 0.25mm in width and 0.2mm in height.

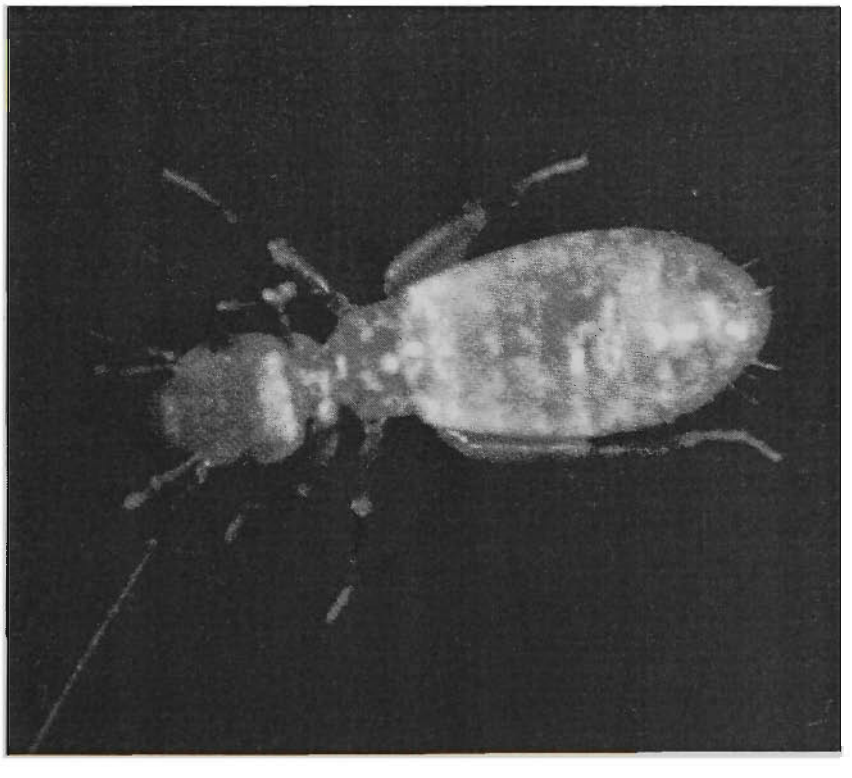

Figure 1.2: Photo of a psocid.

The protection of stored grain from infestation is a complicated problem faced by the grain industry, and to make matters worse there is an ongoing reduction in

the number of chemicals permitted for pest control. Furthermore, resistance to one or more of these chemicals has occurred in most major pest species, and others are currently being phased out due to safety and environmental concerns.

Most Australian cereal grain, oilseeds and pulse crops (>80%), are treated with phosphine (PH_3), which is a low cost and effective fumigant [9]. Phosphine readily disperses in grain bulks and is absorbed in the gaseous state by insects.

The use of chemicals to control insect pests in stored grain is widespread as it is one of the cheapest and simplest means of controlling the major species. However, chemical disinfestation methods suffer from four major problems:

1. sealed structures can be very expensive to fumigate,

2. chemical residues remain within the grain,

3. insects eventually develop resistance to the chemical,

4. it is very difficult to achieve a 100% death rate.

Consequently, a considerable change has occurred in the the attitude of the grain storage industry towards the use of chemical disinfestation methods, and as a result, physical disinfestation methods are gaining popularity as they are typically safer and cleaner. They offer a residue-free alternative with the potential for higher death rates. The most readily available of these is known as *thermal disinfestation*, which involves heating up a grain bulk to a high temperature for a short period of time so that the insects are killed and the grain properties are not significantly affected. For example, Australian grain typically requires heating to approximately 65°C followed

immediately by rapid cooling, to approximately 25°C, in order to achieve satisfactory death rates with effectively no damage to the grain.

Thermal disinfestation offers some of the key attributes of an ideal bulk grain disinfestation process. These include being cheap and fast, offering high death rates, being relatively safe and having minimal impact on the environment. Heat has many advantages, including its rapid effectiveness and the fact it is a well known technology. Large structures and spaces can be treated at temperatures that do not damage equipment. The use of chemicals is not essential but heat can make such treatments more efficient [11]. Heat has been used in conjunction with phosphine and carbon dioxide (CO_2) to enhance the action of the fumigants. Such techniques have been applied to the disinfestation of mills with fairly high levels of kill [9].

With heat disinfestation there exists a *window* of opportunity for most grains between heat dosages that kill insect pests and those which cause significant damage to product quality. If immediate rapid cooling is applied, minimal effects are ensured. The various ways in which grain can be heated to insecticidal temperatures include conduction, convection, fluid bed or sprouted bed, pneumatic conveying, radiative heat, infrared, radio frequency (RF) and microwave radiation [9].

One of the potentially best forms of thermal disinfestation is *heat disinfestation via microwave radiation.* This method is based on exposing an entire bulk of grain to microwave radiation with the principle being that the inherent moisture within the insect is heated by the microwaves. The speed of heating via microwave radiation results in the insects quickly reaching insecticidal temperatures, with the moisture content of the grain, typically between 12% and 14%, not being significantly affected.

The claimed advantages over conventional heat disinfestation methods include:

- fast, as penetration is effectively immediate,
- clean, as no problem with dust, which is messy and combustible,
- potential to kill all stages of insect life,
- potential for smaller sized equipment with lower installation costs,
- potential for selective heating of insects.

The way in which microwave radiation is used to thermally disinfest insects is as follows: energy is absorbed by both the insects and the grain by the electromagnetic field generated, and this in turn produces heat. The water molecules, which are polarized, rotate themselves so that they are orientated with the electric field. The high frequency associated with microwave radiation results in the molecules vibrating in place and hence releasing heat. The heat which is generated depends on such factors as the local concentration of polarised molecules, which means that regions of high moisture will generate greater amounts of heat.

The dielectric properties of a material depend on frequency and vary with temperature and moisture, where the dielectric loss factor is an index of power absorption. The dielectric properties of insects and grain differ, so there exists the possibility of selective heating, whereby the insects are heated to a higher temperature than the grain.

1.2 Mathematically Modelling Heat Transfer in Grain Bulks

Insect behavior, numbers and species are greatly affected by temperature, and by the interstitial relative humidity, hence moisture content, of the grain. Insects are temperature conformers, that is, factors such as their metabolic rate, activity and body temperature depend on the micro-temperature of their surroundings. Thus, infestation is affected by the macroclimate of the region within which the grain is stored, and the microclimate of the grain store.

An understanding of the flow of heat in grain store structures is very important from many industrial perspectives, not just in relation to insect infestation and thermal disinfestation. The heat transfer within the *peripheral layer*, which is the 150mm - 200mm layer of grain in contact with the store structure or the headspace air, is of particular interest. The section of the peripheral layer of most interest is where the grain store structure wall comes into contact with the grain bulk, as illustrated in Figure 1.3, such as along the sides of a silo or the tarpaulin of a *bunker*, which is a simple sealable grain store whereby a heap of grain lying on the ground is covered by tarpaulin. This is where considerable diurnal temperature fluctuation occurs, and where some of the major grain storage problems exist, which include:

- the influence of *aeration*, which is the pumping of ambient air through a static grain bulk [19], within such regions is relatively low. Aeration is used for two main purposes: drying and cooling. Drying is used to reduce the moisture content of grain that is too wet and cooling is used to reduce the temperature

of grain that is too hot [19].

- *passive* heat disinfestation tends to occur within such regions when they are exposed to long periods of heat, from such sources as sunlight. This can lead to excessively high grain temperatures which can result in an unwanted decrease in the moisture content of the grain.

- insect pests, particularly psocids, have been observed to enjoy dwelling within these regions, in what is believed to be a response to the fluctuating temperatures. They move quickly in and out of such regions when the temperature becomes too hot or too cold.

- the *caking* of grain, whereby a *crust* or *mould* forms on the surface of the grain bulk due to the accumulation of moisture.

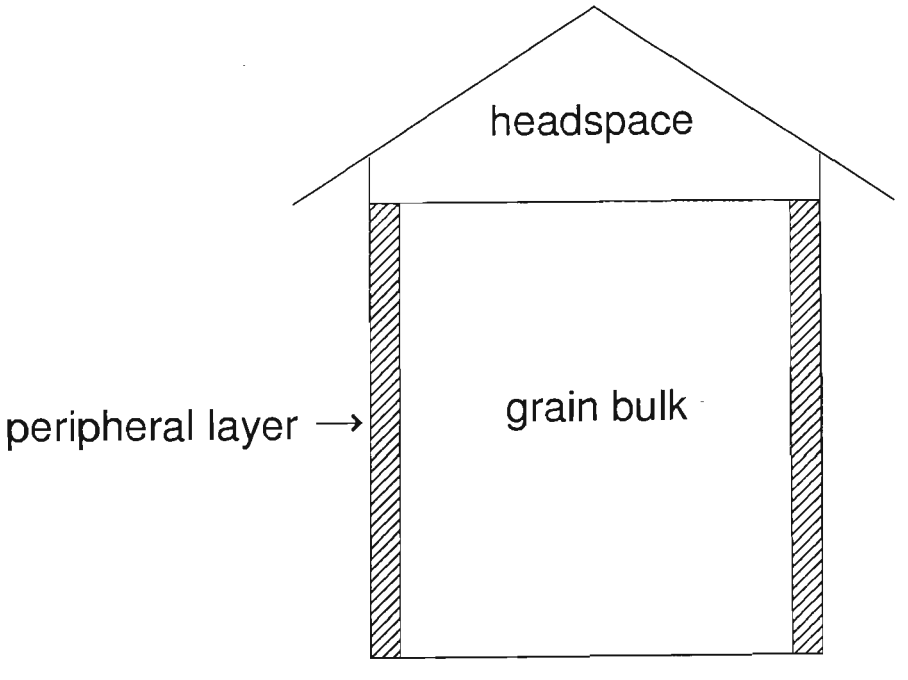

Figure 1.3: The peripheral layer.

Many industrial problems occur within such regions of the peripheral layer, so an understanding of the difference between the air and grain temperatures is very important. For instance, with psocids, understanding the heat transfer on the surface of the grain kernel and within its vicinity, will allow a better understanding of the observed behavior of these insects, and may allow predictions to be made of insect activity which could lead to application of pest control methods being timed to periods of certain insect activity. The moisture is also an important factor, but we are primarily interested in early time and small spatial scales, where heat fluxes predominantly dominate.

To analyse the heat-transfer within such regions, we develop two mathematical models known as the *double-diffusivity heat transfer model* and the *two-stage heat transfer model*. The grain bulk is composed of predominantly air and grain, so we make this distinction in our models, and accordingly, consider the following three different forms by which heat transfer can take place:

- heat transfer through the air,
- heat transfer through the grain,
- heat transfer between the air and the grain.

Also, as we are primarily interested in small time scales, we do not assume thermal equilibrium between the air and grain. The microscopic configuration of the grain bulk is important to both models for obtaining a well-defined macroscopic description, but they differ in how they identify this microstructure. This *dual-region* approach means that both models take into consideration the fact that the heat

transfer in the grain kernel is different to that through the surrounding interstitial air. The main strengths of using a dual-region model over a single-region model, that simply considers the air and grain as one bulk medium, include:

- it allows for a more realistic temperature profile to be obtained as air and grain are two different media with different heat diffusion properties,
- it allows for the ability to predict air and grain temperatures separately, which is an important issue for trying to solve various microclimatic industrial problems, such as dealing with psocids.

We purposely develop linear and relatively simple non-linear mathematical models so that analytical or semi-analytical approximations can be obtained. This is so that analysis can be done on the governing processes involved in order to provide a better understanding of the heat transfer taking place.

In this work, we develop a semi-analytical approximation by the *Heat-Balance Integral Method* for both general and simplified forms of the double-diffusivity heat transfer model, and compare these with numerical approximations obtained by an explicit finite-difference approach. Very good agreement is obtained between the two approximations for both forms of the model.

We also develop small and large time semi-analytical approximations to the two-stage heat transfer model by Laplace transforms, and compare this with a numerical approximations obtained by implementing the Stehfest [58] algorithm. Very good agreement is obtained between the two approximations. We also compare the double-diffusivity heat transfer and the two-stage heat transfer models, and dis-

cuss fundamental differences in their underlying structures. The approximations obtained for both models allow overall variation in temperature of the air and grain to be calculated, in particular, close to the grain store wall. Good agreement is obtained between the two models.

In general, the mathematical modelling of microwave heating processes requires a simultaneous solving of Maxwell's equations of electromagnetism coupled with the heat equation, where all electrical, magnetic and thermal properties are non-linearly dependent on the temperature of the medium being heated. The solution to such a complex coupled system of non-linear equations can be very difficult to obtain, either analytically or numerically, even if sufficient data exists for the various electrical and magnetic properties.

In this work, we reduce the problem to one which involves studying the double-diffusivity heat transfer model, which we develop, with an appended non-linear body heating source term that accounts for heating due to microwave radiation. The model we develop is known as the *double-diffusivity heat transfer model incorporating microwave heating.* A semi-analytical approximation is obtained via the Heat-Balance Integral Method and is compared to a numerical solution obtained from an explicit finite-difference approach. Again, very good agreement is obtained between the two approximations.

The first two mathematical models (the double-diffusivity heat transfer and the two-stage heat transfer models) are very important as no work has previously been done in analysing the difference between the air and grain temperatures within the peripheral layer, either qualitatively or quantitatively. The proposed modelling pro-

vides important insight into the potential difference existing between the air and grain temperatures of a grain bulk, particularly for small time and spatial scales, while the third model (the double-diffusivity heat transfer model incorporating microwave heating) allows us to mathematically predict the air and grain temperature within a grain bulk heated via microwave radiation. All three mathematical models form the foundations for subsequent work to what are very complex practical problems, which we believe will ultimately lead to a better understanding of the microclimate within the peripheral layer of a grain bulk.

1.3 Literature Review

In this section we present a brief overview of literature that relates to the mathematical models developed in this thesis. We begin by first reviewing some of the main dual-region models, and then discuss work related to the mathematical modelling of microwave heating processes.

The double-diffusivity heat transfer model which we develop is based on a heat transfer variant of the theory of *double-diffusivity*. This theory originates from Barenblatt et al. [10], who introduced the concept of a *doubly porous* media when studying seepage in fissured rocks, within the area of petroleum engineering. The fissured rocks were considered to contain an interconnected network of a dual pathway consisting of fissures and porous blocks, with the fissures surrounding the porous blocks. They associated an average pressure with the fissure system and an average pressure with the porous blocks. The fissures were considered to have a high per-

meability and low porosity, while the porous blocks were considered less permeable with a higher porosity. In general, the governing coupled system of equations is of the form

$$\begin{aligned} \frac{\partial P_1}{\partial t} &= D_1 \nabla^2 P_1 - M_1 P_1 + M_2 P_2, \\ \frac{\partial P_2}{\partial t} &= D_2 \nabla^2 P_2 + N_3 P_1 - N_4 P_2, \end{aligned} \tag{1.1}$$

where D_i, M_i, and N_i, $(i = 1, 2)$, are a measure of the porosity, permeability and compressibility and size of the rock, and viscosity and compressibility of the liquid. The rock is considered macroscopically rigid and microscopically compressible, while the liquid is considered compressible with the velocity in both pores and fissures given by Darcy's law.

Aifantis [5] re-derived the governing equations for a doubly porous media (1.1) using the continuum theory of mixtures. He extended this approach by introducing the theory of a *multi-porous media* for which Barenblatt's model is a simplified case. These equations have been derived by Hill [23], among others, from a probabilistic viewpoint by extending the classical random walk model of diffusion.

Rubinstein [54] was one of the first to consider heat conduction in a dual component heterogeneous medium, where an average temperature is considered for each component, and Fourier's law is obeyed in each of the components. The result is a coupled system of equations similar to that of Barenblatt et al. [10].

Hill [25], Aifantis and Hill [7] and Hill and Aifantis [26], developed a *double-diffusivity* model with application to the field of metallurgy, where two possible

diffusion paths were considered. They included the possibility of diffusion along dislocations, grain boundaries, free surfaces or microcracks. Aifantis [5] and Molz [43] applied such an approach to the area of water transport in plants.

Pruess' [51] MINC method is conceptually similar and is a generalisation of Barenblatt's [10] double-porosity concept, which was introduced into petroleum literature by Warren and Root [68], among others, in the form of the double-porosity model. The MINC method is a numerical method for simulating transient non-isothermal, two-phase flow of water in a fractured porous medium.

Babcock et al. [8] developed a model for longitudinal dispersion mechanisms during steady flow of a fluid through unconsolidated spherical beads which include a stagnant fluid film surrounding the particle.

Within the grain literature, there exists a body of work related to the modelling of heat and mass transfer within grain bulks. Most of these models assume equilibrium of local concentration and temperature, and focus on modelling the grain bulk as a whole, and hence tend to be highly complex requiring numerical investigation. Such work includes that done by Sutherland et al. [61], Parry [47], Fohr and Moussa [22], Thorpe and Whitaker [62, 63] and Jia et al. [33, 32].

Both the double-diffusivity heat transfer model and the two-stage heat transfer model are considered *dual-region* models, since they identify the air and grain temperatures within a grain bulk separately. The microscopic configuration of the grain bulk is important to both models for obtaining a well-defined macroscopic description, but they differ in how they identify this microstructure.

The two-stage heat transfer model which we develop is based on McNabb's [40]

two-stage model. Like Barenbalatt et al. [10] (although unaware of Barenblatt's work), McNabb considered the problem of propagation of pressure in a fractured porous medium, with the porous blocks being partitioned by the fissures. However, he identified a specific geometry with the porous blocks, whereby one pressure is associated within the fissures and one within the porous blocks. Neither is averaged over a large number of porous blocks.

Similar models have been used in a number of different areas. Some of the most well known are now briefly discussed.

Skopp and Warrick [55] considered soil particles to be a stationary immobile phase whereby only lateral diffusion occurs, thus acting as a trapping region. Fissures are considered to be a parallel mobile phase. Turner [65] originally considered a trapping phase when modelling flow in packed beds. The trapping regions were dead-water pockets in which diffusion, but not flow, took place.

Skopp and Warrick [55] studied miscible displacement by considering there to be a mobile phase and a stationary phase, whereby solute transfer occurs through the mobile phase via convection, and through the stationary phase via diffusion.

Babcock et al. [8] studied the longitudinal dispersion mechanism of the heat of fluid flow through unconsolidated spherical beads. Convection and diffusion was considered with spherical beads making up the microstructure.

Ma and Lee [37] studied diffusion in porous pellets which were formed from zeolite crystals whereby there were two modes of diffusion, one through the macropore structure between the crystals, and one through the micropore structure within the crystals. The geometry consisted of spheres within spheres. There also exists

applications of the model to the field of medical research, such as Mor et al. [44].

McGuinness [39] extended McNabb's double-porosity model for the pressure response of a naturally fractured reservoir of a single-phase fluid to allow for blocks of varying sizes.

In the field of petroleum engineering, Streltsova-Adams [59] considered similar models which include the interaction between water with gas or oil.

Vortmeyer and Schaefer [67] formulated a dual-region model for an adiabatic packed bed with gas flowing through it. The main difference between this model and the two-stage heat transfer model proposed in this work is that it uses the same coordinate system to describe both the gas and solid phases, and hence assumes an average temperature for the solid phase rather than considering the specific geometry of the solid phase, allowing the temperature to be determined at various points within.

Davis [21] used a two-stage approach based on McNabb [40] to model pyritic oxidation within a waste rock dump, where it is assumed that oxygen transport is the rate-limiting step in the oxidation process. He considers the difference in predictions between a dump assumed to comprise of particles of a single or average size, and a dump where a range of particle sizes is considered. He also discusses the difference between the dual-regions models of Barenblatt et al. [10] and McNabb [40] in relation to the modelling of pyritic oxidation within a waste rock dump, and gives reasons as to why the two-stage approach was used.

We now briefly discuss some other dual-region models, particularly from the groundwater, geothermal and petroleum industries.

Moench [42], in his study of doubly-porous groundwater reservoirs, incorporated the effects of a thin layer of low permeable material or fracture skin which may be present at fracture-block interfaces.

Massoudi and Phuoc [38] developed governing equations for the flow of granular materials between two vertical flat plates set at different temperatures. The assembly consists of spherical particles, densely packed, with natural convection taken into account. The governing equations are derived using a continuum model, which reduces to a system of coupled non-linear ordinary differential equations for a fully developed flow.

Vargas and McCarthy [66] developed a novel Thermal Particle Dynamics (TDP) simulation technique which incorporates both contact mechanics and contact conductance theories in order to model the dynamics of flow and heat conductance through granular materials.

Chen [14] considered the self-heating in a packed particulate that is exothermically reactive. The work focuses on the development of a mathematical model that deals with the hazardous process using milk powder as an example.

Sullivan and Sabersky [60] investigated the convective heat transfer from a flat plate immersed in a flowing granular medium. They devised a semi-analytical model that takes into account the particulate nature of the medium. In such a contact-dominated flow, the motion of the interstitial fluid is not the major means of heat transmission, which is in contrast with the more frequently investigated two-phase systems.

The double-diffusivity heat transfer model incorporating microwave heating de-

veloped in this work is based on extending the double-diffusivity heat transfer model, also developed in this work, by appending a body heating source term to account for heat due to microwave radiation.

Hill and Jennings [28] attempted to model microwave heating processes by solving the heat equation with an assumed form for the heat source due to microwave radiation. In order to identify the body heating source term as accurately as possible, they conducted an exhaustive examination of existing experimental results of Von Hippel [31]. They showed that for different frequencies, particular forms of the body heating source term apply.

Coleman [15, 16], Hill and Smyth [30] as well as Hill and Pincombe [29], adopted the same simplifying approach, in that they ignore the electrical and magnetic aspects explicitly, thus eliminating the need to solve Maxwell's equations, and focused on solving the heat equation with a heat source to account for heat due to microwave radiation. In general, the heat source term used is taken to have either power law or exponential form.

Other authors also attempted to simplify complex problems of modelling microwave heating processes, but their work is based on actually simplifying Maxwell's equations. These include Smyth [56], Kreigsmann et al. [35] and Jolly and Turner [34].

Within the grain literature, there exists a body of work related to experimental investigation of the microwave heating of grain bulks, some of which are infested with insect pests, as done by Trabelsi et al. [64], Nelson [45] and Nelson et al. [46].

1.4 Overview of Thesis

In this thesis, the problem of modelling heat transfer within a grain bulk is investigated using three dual-region heat transfer models.

The first part of the thesis, Chapters 2 and 3, deals with developing the double-diffusivity heat transfer and the dual-region heat transfer models, in order to obtain estimates of the air and grain temperatures within the grain bulk, in particular, within the peripheral layer. The second part of the thesis, Chapter 4, involves examining the heat transfer within a grain bulk exposed to microwave radiation, by developing the double-diffusivity heat transfer model incorporating microwave heating.

In Chapter 2 we illustrate the development of the double-diffusivity heat transfer model. We also outline in detail the implementation of the Heat-Balance Integral Method. We illustrate how we can obtain a simplified form of the double-diffusivity heat transfer model, and show how to obtain a semi-analytical approximation via the Heat-Balance Integral Method for this model. We also consider a general case of the model, and once again illustrate how to obtain a semi-analytical approximation via the Heat-Balance Integral Method. For both models, semi-analytical approximations are compared with numerical approximations obtained via an explicit forward time and central space (FTCS) finite-difference scheme. Very good agreement between the semi-analytical and numerical approximations is obtained. Very good agreement is also obtained between the simplified and general forms of the model. We also show that the position of the moving front is $X \approx C\sqrt{t}$ for early

time, through the air and grain paths, for both the simplified and general forms of the model.

In Chapter 3 we illustrate the development of the two-stage heat transfer model. We obtain a semi-analytical approximation via Laplace transforms valid for small and large times. These semi-analytical approximations are compared with numerical approximations obtained by the Stehfest [58] algorithm. Very good agreement between the semi-analytical and numerical approximations is obtained. We also discuss the theoretical differences between the double-diffusivity heat transfer and the two-stage heat transfer models. We do a qualitative comparison of the two models via some results, and discuss any similarities and differences based on their theoretically fundamental different structures. Good agreement is obtained between the two models.

In Chapter 4 we illustrate the development of the double-diffusivity heat transfer model incorporating microwave heating. We obtain a semi-analytical approximation via the Heat-Balance Integral Method, and compare this with numerical results obtained by an explicit FTCS finite-difference scheme. Again, very good agreement between the semi-analytical and numerical approximations is obtained. These results are compared to those of Chapter 2 to illustrate the difference between a grain bulk which is heated via ambient air and one that is heated via microwave radiation.

In Chapter 5 we present our conclusions.

Chapter 2

The Double-Diffusivity Heat Transfer Model

2.1 Introduction

In this chapter we develop the double-diffusivity heat transfer model. We illustrate how to obtain a semi-analytical approximation to this model by the Heat-Balance Integral Method. We also apply this method to a simplified form of the model which can be decoupled, allowing us to obtain semi-analytical approximations for the air and grain temperatures independently. We compare these approximations to numerical approximations obtained via an explicit finite-difference scheme.

2.2 Mathematical Formulation

We first illustrate the derivation of the double-diffusivity model via a random-walk approach as proposed by Hill [23], followed by the development of the continuous version of this model. We then derive our heat transfer variant of this model, known as the double-diffusivity heat transfer model.

2.2.1 Derivation of the Double-Diffusivity Model

It is well known that to describe the diffusion in a homogeneous, isotropic, isothermal, rigid medium with a single family of diffusion paths, the classical diffusion equation, based on Fick's second law of diffusion, is used,

$$\frac{\partial C}{\partial t} = D\nabla^2 C, \quad D > 0, \tag{2.1}$$

where C is the concentration and D the diffusion coefficient.

The question is, how does one model diffusion in a medium where there exist two distinct diffusion paths? Aifantis [4] has proposed the following general coupled system of equations for the concentrations in each path:

$$\begin{aligned} \frac{\partial C_1}{\partial t} &= D_1\nabla^2 C_1 - K_1 C_1 + K_2 C_2, \\ \frac{\partial C_2}{\partial t} &= D_2\nabla^2 C_2 + K_1 C_1 - K_2 C_2, \end{aligned} \tag{2.2}$$

where D_1 and D_2 are the positive diffusion coefficients, and K_1 and K_2 are the positive concentration transfer coefficients. This coupled system is known as the *double-diffusivity model.* Formally, similar equations have been proposed by Hill [23], and originate from Barenblatt et al. [10], where they were developed to describe the

flow of liquid in rocks assumed to consist of a dual system of fissures and pores. This theory describes diffusion and flow in a medium that consists of more than one family of diffusion or flow paths. Thus, such a theory is directly applicable to the seepage of water in soils where additional flow paths arise, such as from the cracking of the soil.

In order to show the derivation of the double-diffusivity model, we will consider a random-walk approach. Following, we detail the discrete random walk model giving rise to the classical diffusion equation (2.1) (see Prabhu [50]). Consider a particle random walking on the integers, such that at integral instants in time, there is a probability of p for a move to the right, and a probability of q for a move to the left, where $p+q=1$. If we let $u_{k,n}$ denote the probability that the particle is in position k at time n, then, for an unrestricted particle

$$u_{k,n+1} = pu_{k-1,n} + qu_{k+1,n}, \quad \forall n \geq 0. \tag{2.3}$$

If we now let the jumps be of length Δx with the time interval between jumps Δt, then in the limit as Δx and Δt tend to zero, $u_{k,n}$ is approximately equal to $f(x,t)dx$ and equation (2.3) becomes

$$f(x,t+\Delta t) = pf(x-\Delta x,t) + qf(x+\Delta x,t). \tag{2.4}$$

From Taylor's theorem, we have

$$\Delta t\frac{\partial f}{\partial t} = \frac{(p+q)}{2}(\Delta x)^2\frac{\partial^2 f}{\partial x^2} - (p-q)\Delta x\frac{\partial f}{\partial x}, \tag{2.5}$$

hence, for a free particle ($p=q=1/2$), we obtain the classical diffusion equation (2.1), provided Δt and Δx converge to zero in such a way that $\Delta t/(\Delta x)^2$ tends to the finite limit $(2D)^{-1}$.

We now illustrate the development of the double-diffusivity model using a discrete random walk model of diffusion in a medium with two distinct diffusion paths. This model gives rise to the double-diffusivity model (2.2) in the continuous limit, which is derived in the next section. The idea behind the random walk approach of the double-diffusivity model is to generalise the above classical method by assuming that the particle moves along one of two distinct paths and that at each jump there is a possibility that it can transfer between the two paths, in addition to moving either right or left.

Consider a single particle random walking on the integers on an infinite straight line. We make the idealisation that each point of space is simultaneously occupied by two distinct diffusion or flow paths. Thus, we consider the infinite line to consist of two paths. If the particle is in path i, where $i = 1, 2$, we suppose that at each jump it moves one step to the right with probability p_i, one step to the left with probability q_i, remains in the same position with probability r_i, or jumps to the same position on the other path with probability s_i, as illustrated in Figure 2.1.

At each jump only one of four possible outcomes can occur, thus

$$p_i + q_i + r_i + s_i = 1, \quad i = 1, 2, \tag{2.6}$$

and we assume that the various probabilities are independent of the position of the particle.

We now let $u_{k,n}$ denote the probability that the particle is in path 1 at position k at time step n. Similarly, let $v_{k,n}$ denote the probability that the particle is in path 2 at position k at time step n. We thus have the following coupled system of

equations,

$$\begin{aligned} u_{k,n+1} &= p_1 u_{k-1,n} + r_1 u_{k,n} + q_1 u_{k+1,n} + s_2 v_{k,n}, \\ v_{k,n+1} &= p_2 v_{k-1,n} + r_2 v_{k,n} + q_2 v_{k+1,n} + s_1 u_{k,n}, \end{aligned} \tag{2.7}$$

$\forall k, n \in \mathrm{Z} \geq 0$.

We now illustrate how the continuous version of the random walk model (2.7) gives rise to the coupled system of partial differential equations (2.2) in the case of a free particle, that is, $p_i = q_i$, $i = 1, 2$.

Let the length of each step be Δx and the time between consecutive steps be Δt. Formally, we replace k and n by x and t, respectively, and introduce functions $f(x,t)$ and $g(x,t)$ such that in the limit of Δx and Δt tending to zero, $u_{k,n}$ and $v_{k,n}$ are approximately $f(x,t)dx$ and $g(x,t)dx$, respectively.

The corresponding equations to the system of equation (2.7) are

$$\begin{aligned} f(x, t+\Delta t) &= p_1 f(x-\Delta x, t) + r_1 f(x,t) + q_1 f(x+\Delta x, t) + s_2 g(x,t), \\ g(x, t+\Delta t) &= p_2 g(x-\Delta x, t) + r_2 g(x,t) + q_2 g(x+\Delta x, t) + s_1 f(x,t). \end{aligned} \tag{2.8}$$

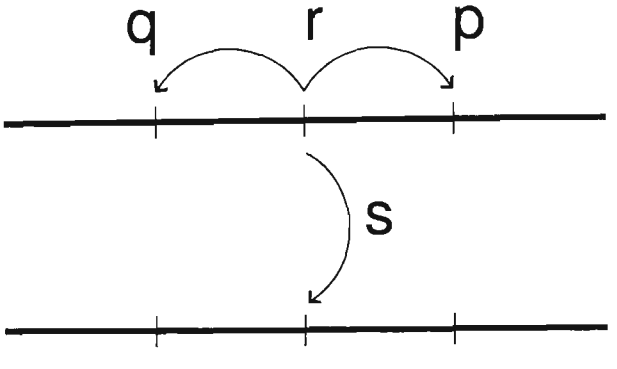

Figure 2.1: The random walk of a particle.

Up to first order in Δt and second order in Δx, the system of equations (2.8) becomes

$$\begin{aligned} \Delta t \frac{\partial f}{\partial t} &= \frac{(p_1+q_1)}{2}(\Delta x)^2 \frac{\partial^2 f}{\partial x^2} - (p_1-q_1)\Delta x \frac{f}{x} - s_1 f + s_2 g, \\ \Delta t \frac{\partial g}{\partial t} &= \frac{(p_2+q_2)}{2}(\Delta x)^2 \frac{\partial^2 g}{\partial x^2} - (p_2-q_2)\Delta x \frac{g}{x} - s_2 g + s_1 f, \end{aligned} \tag{2.9}$$

using equation (2.6).

By supposing Δt and Δx tend to zero in such a way that $\Delta t/(\Delta x)^2$ tends to a finite positive limit λ, and assuming that the probabilities p_i, q_i, s_i, $i = 1, 2$ are such that

$$p_i = \lambda(D_i + d_i \Delta x), \quad q_i = \lambda(D_i - d_i \Delta x) \text{ and } s_i = \lambda k_i (\Delta x)^2, \tag{2.10}$$

where d_i, D_i and k_i, $i = 1, 2$ are assumed to be finite constants, then from equations (2.9) and (2.10), we obtain

$$\begin{aligned} \frac{\partial f}{\partial t} &= D_1 \frac{\partial^2 f}{\partial x^2} - 2d_1 \frac{\partial f}{\partial x} - k_1 f + k_2 g, \\ \frac{\partial g}{\partial t} &= D_2 \frac{\partial^2 g}{\partial x^2} - 2d_2 \frac{\partial g}{\partial x} - k_2 g + k_1 f. \end{aligned} \tag{2.11}$$

In the case of a free particle, $p_i = q_i$, $i = 1, 2$, we obtain the double-diffusivity model (2.2) and we observe that the constants k_1 and k_2 are essentially transition probabilities.

2.2.2 Derivation of the Double-Diffusivity Heat Transfer Model

Now that we have outlined the derivation of the double-diffusivity model, we illustrate our heat transfer variant of the model, namely, the double-diffusivity heat transfer model. The fundamental assumption behind this model is that each point

within the grain bulk is occupied by *both* air and grain. This idealisation is based on the random distribution of grain throughout the grain bulk, and as it is not known if a particular point is occupied by either air or grain, we make the idealisation that each point is occupied by both, and obtain the actual temperature at that point by taking the average of the two temperatures. Such a model is well suited to the problem of determining the difference in the air and grain temperatures within a grain bulk, as their distribution is random in nature. We also assume that the dust contained within the grain bulk does not significantly affect heat transfer. It would be possible to develop a *triple-diffusivity heat transfer model* which considers the dust, or some other medium, as a third diffusivity path for the heat.

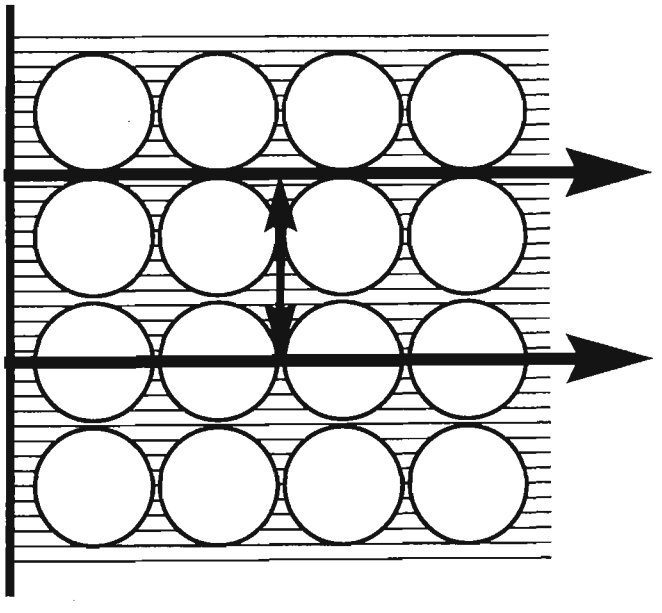

Figure 2.2: Idealisation of the double-diffusivity heat transfer model.

The scenario which we consider is that of a closely packed grain bulk in contact with the vertical grain store wall such that every point in the grain bulk is connected to every other point by either a grain path or by an air path, and we envisage heat

propagating along both air and grain paths, as illustrated in Figure 2.2. The heat transfer through the grain path occurs through the grain kernels via the grain contact areas, and the heat transfer through the air path occurs through the air channels created by the pores. At every point within the grain bulk we associate both an air temperature $T_a(x,t)$ and a grain temperature $T_g(x,t)$, such that the actual physical temperature at that point is simply the average, or the weighted average, of the two. In addition to heat propagating along the air and grain paths, we speculate that there can be transfer of heat from air to grain, and vice-versa. The heat transfer within the peripheral layer is most critical when internal convection cells are not fully established. Convective currents are thus assumed to be negligible to allow such situations to be analysed.

Analogously to the derivation of the double-diffusivity model, we obtain the one-dimensional double-diffusivity heat transfer model

$$\begin{aligned} \frac{\partial T_a(x,t)}{\partial t} &= K_a \frac{\partial^2 T_a(x,t)}{\partial x^2} - k_1 T_a(x,t) + k_1 T_g(x,t), \\ \frac{\partial T_g(x,t)}{\partial t} &= K_g \frac{\partial^2 T_g(x,t)}{\partial x^2} + k_2 T_a(x,t) - k_2 T_g(x,t), \end{aligned} \tag{2.12}$$

where the coupling terms between the air and grain paths are defined as follows

$$k_1 = \frac{k_a}{\rho_a c_a} \quad \text{and} \quad k_2 = \frac{k_a}{\rho_g c_g}, \tag{2.13}$$

and where T_a is the temperature of the air, T_g is the temperature of the grain, K_a is the thermal diffusivity of the air and K_g is the thermal diffusivity of the grain. We use k_a to represent the *effective* heat transfer coefficient from air to grain or grain to air, across some area.

Another method for deriving the double-diffusivity heat transfer model (2.12) is as follows. Consider the general one-dimensional heat equation with a source/sink term Q:

$$\rho c \frac{\partial U}{\partial t} = \kappa \frac{\partial^2 U}{\partial x^2} + Q, \tag{2.14}$$

where Q is the rate of heat produced/lost per unit volume per unit time. Now, if Q represents heat lost/gained through Newton cooling, that is,

$$Q \approx hA\left(U(x,t) - U_s\right), \tag{2.15}$$

where h is the heat transfer coefficient, A is the cross-sectional area and U_s is the surrounding temperature, then, by adapting this to the double-diffusivity model approach, we obtain the following coupled system

$$\begin{aligned} \rho_a c_a \frac{\partial T_a}{\partial t} &= \kappa_a \frac{\partial^2 T_a}{\partial x^2} - hA\left(T_a - T_g\right), \\ \rho_g c_g \frac{\partial T_g}{\partial t} &= \kappa_g \frac{\partial^2 T_g}{\partial x^2} + hA\left(T_a - T_g\right), \end{aligned} \tag{2.16}$$

where we consider the air to act as a source of heat for the grain, since air heats up faster than grain, which is equivalent to

$$\begin{aligned} \frac{\partial T_a}{\partial t} &= K_a \frac{\partial^2 T_a}{\partial x^2} - \frac{hA}{\rho_a c_a} T_a + \frac{hA}{\rho_a c_a} T_g, \\ \frac{\partial T_g}{\partial t} &= K_g \frac{\partial^2 T_g}{\partial x^2} + \frac{hA}{\rho_g c_g} T_a - \frac{hA}{\rho_g c_g} T_g, \end{aligned} \tag{2.17}$$

and by letting $k_a = hA$, we obtain the double-diffusivity heat transfer model (2.12).

2.3 The Heat-Balance Integral Method

In this section we discuss the implementation of the Heat-Balance Integral Method (HBIM).

The HBIM is commonly used to obtain semi-analytical approximations to problems involving heat conduction and diffusion. The HBIM is based on the existence of a *penetration depth*, denoted $X(t)$, beyond which there is effectively no heat flow. Such a solution technique is very well suited to our problem, as such penetration depths exist in grain bulks and are readily observed in the field.

In particular, it is a very good technique to obtain semi-analytical approximations to non-linear transient heat equation problems. It can also be used for obtaining approximate solutions to linear problems with complicated spatially-dependent thermal properties, and problems involving both conduction and convection.

Pohlhousen [48] was one of the first to introduce integral methods, and used them to solve non-similar boundary layer problems in fluid mechanics. The first to apply the method to solve diffusion equations was Landahl [36] in the field of biophysics.

The implementation of the HBIM basically comprises of four steps [27]:

1. Begin by introducing the notion of a *penetration depth*, $X(t)$, beyond which there is effectively no heat flow, as illustrated in Figure 2.3. This is analogous to the boundary layer thickness in fluid mechanics.

2. Assume a simple polynomial profile for the temperature in the spatial variable with time-dependent coefficients.

3. Use the prescribed initial conditions and boundary conditions, along with the assumed conditions beyond the penetration depth, to determine the coefficients of the assumed polynomial temperature profile.

4. Integrate the governing equation across the penetration depth, to obtain what is known as the *heat-balance integral*, and from the assumed temperature profile determine $X(t)$ explicitly from the integrated form of the governing equation. Hence, the temperature will satisfy the heat-balance integral, but not the original governing equation. Thus, the governing equation will be satisfied in an *averaged* or integral sense only. This averaged equation is analogous to the momentum integral in boundary layer theory.

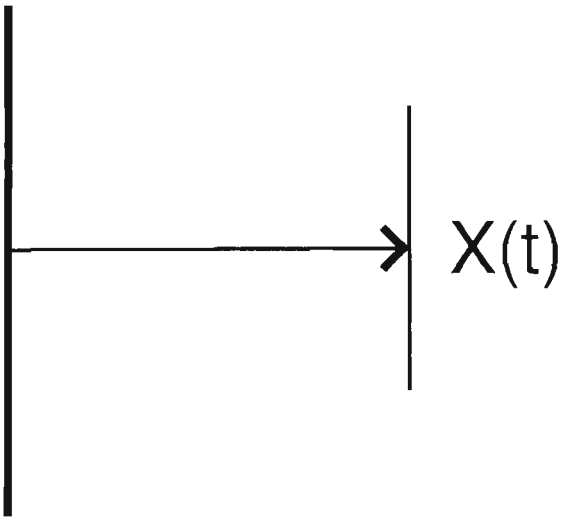

Figure 2.3: Idealisation of the penetration depth.

In our implementation of the HBIM to the double-diffusivity heat transfer model and the double-diffusivity heat transfer model incorporating microwave heating in Chapter 4, we assume the existence of two penetration depths, one through the air path $X_a(t)$, the other through the grain path $X_g(t)$, which vary with time,

and beyond which there is effectively no heat flow. In addition, we assume cubic temperature profiles for both the air and grain. Ordinary differential equations for the moving penetration fronts are then determined by satisfying the governing partial differential equations in an average or integral sense.

2.4 A Semi-Analytical Approximation via the HBIM to the General Double-Diffusivity Heat Transfer Model

In this section we illustrate the derivation of a semi-analytical approximation to the general double-diffusivity heat transfer model (2.12) using the HBIM.

We begin by determining expressions for $T_a(x,t)$ and $T_g(x,t)$, which are functions of $X_a(t)$ and $X_g(t)$. We then determine the coupled governing equations for the penetration fronts $X_a(t)$ and $X_g(t)$.

We will first determine an expression for $T_a(x,t)$. We assume that there exists a penetration depth $x = X_a(t)$ beyond which there is effectively no heat flow. Thus, at $x = X_a(t)$, we have

$$\begin{aligned} T_a &= T_{a0}, \\ \frac{\partial T_a}{\partial x} &= 0, \end{aligned} \tag{2.18}$$

since both temperature and heat flux must be continuous. Note that T_{a0} is the initial temperature of the air, and as such is the internal temperature at the penetration

point $x = X_a$.

Now, let us consider T_a at $x = X_a$. Upon differentiating both sides of equation $(2.18)_1$ with respect to time, we find

$$X_a' \frac{\partial T_a}{\partial x} + \frac{\partial T_a}{\partial t} = 0, \tag{2.19}$$

where primes indicate derivatives with respect to t.

Hence, from equation $(2.18)_2$, we obtain

$$\frac{\partial T_a}{\partial t}(X_a, t) = 0. \tag{2.20}$$

Thus, at $x = X_a$, equation $(2.12)_1$ becomes

$$K_a \frac{\partial^2 T_a}{\partial x^2} - k_1 T_a + k_1 T_g = 0, \tag{2.21}$$

and so, from equation $(2.18)_1$, we obtain

$$\frac{\partial^2 T_a}{\partial x^2}(X_a, t) = \frac{k_1}{K_a} T_{a0} - \frac{k_1}{K_a} T_g(X_a, t), \tag{2.22}$$

which is a derived constraint. Hence, we have four conditions on T_a:

$$\begin{aligned} &T_a(0,t) = T_b, \qquad T_a(X_a,t) = T_{a0}, \\ &\frac{\partial T_a}{\partial x}(X_a,t) = 0, \qquad \frac{\partial^2 T_a}{\partial x^2}(X_a,t) = \frac{k_1}{K_a} T_{a0} - \frac{k_1}{K_a} T_g(X_a,t), \end{aligned} \tag{2.23}$$

where $T_b(t)$ is the boundary temperature.

We now assume a cubic temperature profile for T_a in the spatial variable, with time-dependent coefficients:

$$T_a(x,t) = a(t) + b(t)x + c(t)x^2 + d(t)x^3, \tag{2.24}$$

and determine the values of the time-dependent coefficients using equations (2.23). We choose a cubic so there are four free parameters to match our four boundary conditions, one each for T_a and T_g at $x = 0$ and $x = \infty$.

Using equations (2.23), we obtain the following expressions for the four time-dependent coefficients

$$\begin{aligned} a &= T_b, \\ b &= \frac{3}{X_a}T_{a0} - \frac{3}{X_a}T_b + \frac{k_1 X_a}{2K_a}T_{a0} - \frac{k_1 X_a}{2K_a}T_g(X_a,t), \\ c &= -\frac{3}{X_a^2}T_{a0} + \frac{3}{X_a^2}T_b - \frac{k_1}{K_a}T_{a0} + \frac{k_1}{K_a}T_g(X_a,t), \\ d &= \frac{T_{a0}}{X_a^3} - \frac{T_b}{X_a^3} + \frac{k_1}{2K_a X_a}T_{a0} - \frac{k_1}{2K_a X_a}T_g(X_a,t). \end{aligned} \tag{2.25}$$

Hence, upon substituting (2.25) into equation (2.24), the expression for T_a becomes

$$\begin{aligned} T_a(x,t) &= T_{a0} + (T_b - T_{a0})\left(1 - \frac{x}{X_a}\right)^3 \\ &+ (k_1 T_{a0} - k_1 T_g(X_a,t))\left(\frac{X_a x}{2K_a} - \frac{x^2}{K_a} + \frac{x^3}{2K_a X_a}\right). \end{aligned} \tag{2.26}$$

Initially ($t = 0$) it is assumed that

$$T_{a0} = T_{g0}, \tag{2.27}$$

so by letting $T_{a0} = T_{g0} = T_0$, the expression for T_a becomes:

$$\begin{aligned} T_a(x,t) &= T_0 + (T_b - T_0)\left(1 - \frac{x}{X_a}\right)^3 \\ &- \frac{k_1 X_a x}{2K_a}(T_g(X_a,t) - T_0)\left(1 - \frac{x}{X_a}\right)^2. \end{aligned} \tag{2.28}$$

Analogously, by assuming a penetration depth $x = X_g(t)$, we obtain the following expression for T_g:

$$\begin{aligned} T_g(x,t) &= T_0 + (T_b - T_0)\left(1 - \frac{x}{X_g}\right)^3 \\ &- \frac{k_2 X_g x}{2K_g}(T_a(X_g,t) - T_0)\left(1 - \frac{x}{X_g}\right)^2. \end{aligned} \tag{2.29}$$

Once expressions for X_a and X_g are determined, explicit expressions for T_a and T_g will exist, given by equations (2.28) and (2.29).

We now let

$$\Phi_a(t) = \int_0^{X_a} T_a \, dx, \tag{2.30}$$

where Φ_a is simply some function of t, so that equation $(2.12)_1$ will be satisfied in an averaged or integral sense over the interval $[0, X_a]$. Upon differentiating both sides with respect to time, we have

$$\frac{d\Phi_a}{dt} = \int_0^{X_a} \frac{\partial T_a}{\partial t} \, dx + T_a(X_a,t)X_a'. \tag{2.31}$$

Thus, from equations $(2.12)_1$, $(2.18)_1$ and $(2.18)_2$, we obtain the following expression which becomes the governing expression for $X_a(t)$:

$$\frac{d\Phi_a}{dt} = -K_a \frac{\partial T_a}{\partial x}(0,t) - k_1\Phi_a + k_1 \int_0^{X_a} T_g \, dx + T_0 X_a'. \tag{2.32}$$

We must now determine expressions for

$$\Phi_a, \quad \frac{\partial T_a}{\partial x}(0,t) \text{ and } \int_0^{X_a} T_g\, dx. \tag{2.33}$$

Upon differentiating equation (2.28) with respect to x, we obtain

$$\frac{\partial T_a}{\partial x}(0,t) = -\frac{3}{X_a}(T_b - T_0) - \frac{k_1 X_a}{2K_a}(T_g(X_a,t) - T_0). \tag{2.34}$$

By using the expression for T_a, that is, equation (2.28), equation (2.30) becomes

$$\Phi_a = T_0 X_a + \frac{X_a}{4}(T_b - T_0) - \frac{X_a^3 k_1}{24K_a}(T_g(X_a,t) - T_0). \tag{2.35}$$

Finally, from equation (2.18), we obtain

$$\begin{aligned} \int_0^{X_a} T_g\, dx &= T_b X_a + \frac{X_a^2}{X_g}(T_b - T_0)\left(-\frac{3}{2} + \frac{X_a}{X_g} - \frac{X_a^2}{4X_g^2}\right) \\ &- \frac{k_2 X_g X_a^2}{2K_g}(T_a(X_g,t) - T_0)\left(\frac{1}{2} - \frac{2X_a}{3X_g} + \frac{X_a^2}{4X_g^2}\right). \end{aligned} \tag{2.36}$$

thus, equation (2.32) becomes

$$\frac{X_a'}{4}(T_b - T_0) + \frac{X_a}{4}T_b' - \frac{k_1 X_a^3}{24K_a}\frac{d}{dt}T_g(X_a,t)$$

$$- \frac{k_1 X_a^2 X_a'}{8K_a}(T_g(X_a,t) - T_0)$$

$$= (T_b - T_0)\left(\frac{3K_a}{X_a} - \frac{k_1 X_a}{4}\right)$$

$$+ (T_b - T_0)\frac{k_1 X_a^2}{X_g}\left(-\frac{3}{2} + \frac{X_a}{X_g} - \frac{X_a^2}{4X_g^2}\right) \tag{2.37}$$

$$+ \quad (T_g(X_a,t)-T_0)\frac{k_1}{2}\left(X_a+\frac{k_1X_a^3}{12K_a}\right)$$

$$+ \quad (T_a(X_g,t)-T_0)\frac{k_1k_2X_a^2}{K_g}\left(-\frac{X_g}{4}+\frac{X_a}{3}-\frac{X_a^2}{8X_g}\right)$$

$$+ \quad X_a(k_1T_b-k_1T_0).$$

It follows then, from using the fact that at $x = X_a$, we have

$$\frac{d}{dt}T_g(x,t)=\frac{\partial T_g}{\partial x}X_a^{'}+\frac{\partial T_g}{\partial t}, \tag{2.38}$$

and given that $T_{a0} = T_{g0} = T_0$, from equation (2.27), that the governing equation for X_a becomes

$$\begin{aligned}
&T_b^{'}X_a+X_a^{'}(T_b-T_0)-\frac{\partial T_g}{\partial x}(X_a,t)\frac{X_a^{'}X_a^3k_1}{6K_a}\\
&-\frac{\partial T_g}{\partial t}(X_a,t)\frac{k_1X_a^3}{6K_a}-(T_g(X_a,t)-T_0)\frac{k_1X_a^2X_a^{'}}{2K_a}\\
&=(T_b-T_0)\left(\frac{12K_a}{X_a}-k_1X_a\right)\\
&+(T_b-T_0)4k_1X_a\left(1-\frac{3X_a}{2X_g}+\frac{X_a^2}{X_g^2}-\frac{X_a^3}{4X_g^3}\right)\\
&+(T_g(X_a,t)-T_0)2k_1X_a\left(1+\frac{k_1X_a^2}{12K_a}\right)\\
&+(T_a(X_g,t)-T_0)\frac{4k_1k_2X_a^2}{K_g}\left(\frac{X_a}{3}-\frac{X_g}{4}-\frac{X_a^2}{8X_g}\right).
\end{aligned} \tag{2.39}$$

Similarly, we obtain the following expression for the governing equation for X_g,

$$\begin{aligned}
& T_b' X_g + X_g'(T_b - T_0) - \frac{\partial T_a}{\partial x}(X_g, t)\frac{X_g' X_g^3 k_2}{6K_g} \\
- & \frac{\partial T_a}{\partial t}(X_g, t)\frac{k_2 X_g^3}{6K_g} - (T_a(X_g, t) - T_0)\frac{k_2 X_g^2 X_g'}{2K_g} \\
= & (T_b - T_0)\left(\frac{12K_g}{X_g} - k_2 X_g\right) \\
+ & (T_b - T_0)4k_2 X_g\left(1 - \frac{3X_g}{2X_a} + \frac{X_g^2}{X_a^2} - \frac{X_g^3}{4X_a^3}\right) \\
+ & (T_a(X_g, t) - T_0)2k_2 X_g\left(1 + \frac{k_2 X_g^2}{12K_g}\right) \\
+ & (T_g(X_a, t) - T_0)\frac{4k_1 k_2 X_g^2}{K_a}\left(\frac{X_g}{3} - \frac{X_a}{4} - \frac{X_g^2}{8X_a}\right).
\end{aligned} \tag{2.40}$$

We now assume that one of the penetration fronts moves faster than the other, such as $X_a > X_g$, which then implies $T_g(X_a, t) = T_{g0}$, as can be seen in Figure 2.4. This assumption is reasonable, since the double-diffusivity approach is typically applied to problems in which there not only exist two diffusion paths, but there is at least one order of magnitude difference in the rate of diffusion within the two paths. For our scenario, the difference is approximately two orders of magnitude, as discussed in Section 2.5. This assumption, along with the fact $T_{a0} = T_{g0} = T_0$, from equation (2.27), results in the governing equations for X_a and X_g, equations (2.39)

and (2.40), respectively, simplifying as follows:

$$\begin{aligned} & T_b^{'} X_a + X_a^{'}(T_b - T_0) - \frac{\partial T_g}{\partial t}(X_a, t)\frac{k_1 X_a^3}{6K_a} \\ = \; & (T_b - T_0)\left(\frac{12K_a}{X_a} - k_1 X_a\right) \\ + \; & (T_b - T_0)4k_1 X_a\left(1 - \frac{3X_a}{2X_g} + \frac{X_a^2}{X_g^2} - \frac{X_a^3}{4X_g^3}\right) \\ + \; & (T_a(X_g, t) - T_0)\frac{4k_1 k_2 X_a^2}{K_g}\left(\frac{X_a}{3} - \frac{X_g}{4} - \frac{X_a^2}{8X_g}\right), \end{aligned} \tag{2.41}$$

and

$$\begin{aligned} & T_b^{'} X_g + X_g^{'}(T_b - T_0) - \frac{\partial T_a}{\partial x}(X_g, t)\frac{X_g^{'} X_g^3 k_2}{6K_g} \\ - \; & \frac{\partial T_a}{\partial t}(X_g, t)\frac{k_2 X_g^3}{6K_g} - (T_a(X_g, t) - T_0)\frac{k_2 X_g^2 X_g^{'}}{2K_g} \\ = \; & (T_b - T_0)\left(\frac{12K_g}{X_g} - k_2 X_g\right) \\ + \; & (T_b - T_0)4k_2 X_g\left(1 - \frac{3X_g}{2X_a} + \frac{X_g^2}{X_a^2} - \frac{X_g^3}{4X_a^3}\right) \\ + \; & (T_a(X_g, t) - T_0)2k_2 X_g\left(1 + \frac{k_2 X_g^2}{12K_g}\right). \end{aligned} \tag{2.42}$$

It is worth noting the appearance of the heat driving terms within the coupled system of penetration fronts $X_a(t)$ and $X_g(t)$, equations (2.41) and (2.42). These

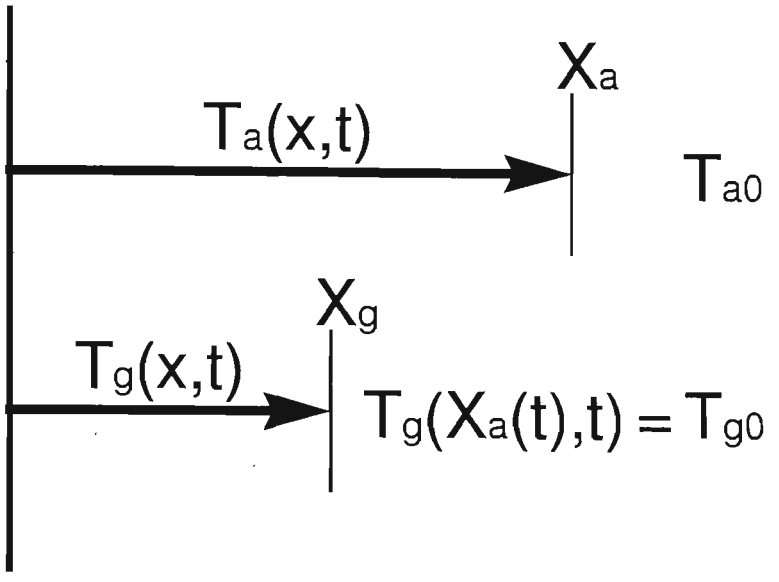

Figure 2.4: Idealisation of the assumption that $X_a > X_g$.

terms are of the form

$$T_b - T_0 \quad \text{and} \quad T_a(X_g, t) - T_0. \tag{2.43}$$

This is in agreement with what we expect, as it illustrates the importance of the difference between the boundary temperature and the initial temperature, as well as the difference between the temperature at the penetration front and the initial internal temperature, which contribute to the rate at which the heat propagates through the medium.

In order to obtain expressions for X_a and X_g, the coupled system of equations (2.41) and (2.42), must be solved. Due to the complexity of these expressions, this must be done numerically. The values of X_a and X_g are then substituted into equations (2.28) and (2.29), enabling expressions for T_a and T_g to be obtained.

Applying the simplification $T_g(X_a, t) = T_{g0}$, the expression for T_a becomes

$$T_a(x,t) = T_0 + (T_b - T_0)\left(1 - \frac{x}{X_a}\right)^3, \tag{2.44}$$

while the expression for T_g, equation (2.29), remains unchanged.

2.4.1 Showing that $X(t) \approx C\sqrt{t}$ for Early Times

In this section we show that $X(t) \approx C\sqrt{t}$, for early time.

We substitute $X_a = C_1\sqrt{t}$ and $X_g = C_2\sqrt{t}$, where C_1 and C_2 are constants, into the governing equations for X_a and X_g, equations (2.41) and (2.42), and retain terms of $O(t^{1/2})$.

We then obtain the following values for C_1 and C_2,

$$C_1 = 2\sqrt{6K_a} \quad \text{and} \quad C_2 = 2\sqrt{6K_g}. \tag{2.45}$$

Therefore, the expressions for the penetration fronts $X_a(t)$ and $X_g(t)$, at early times, are, respectively,

$$X_a(t) = 2\sqrt{6K_a}\sqrt{t}, \tag{2.46}$$

$$X_g(t) = 2\sqrt{6K_g}\sqrt{t}. \tag{2.47}$$

By substituting these expressions into equations (2.44) and (2.29), we obtain the following expressions for $T_a(x,t)$ and $T_g(x,t)$ at early times, respectively,

$$T_a(x,t) = T_0 + (T_b - T_0)\left(1 - \frac{x}{2\sqrt{6K_a}\sqrt{t}}\right)^3, \tag{2.48}$$

$$\begin{aligned} T_g(x,t) &= T_0 + (T_b - T_0)\left(1 - \frac{x}{2\sqrt{6K_g}\sqrt{t}}\right)^3 \\ &- \frac{xk_2\sqrt{6}\sqrt{t}}{\sqrt{K_g}}(T_b - T_0)\left(1 - \frac{x}{2\sqrt{6K_g}\sqrt{t}}\right)^2\left(1 - \frac{\sqrt{K_g}}{\sqrt{K_a}}\right)^3. \end{aligned} \tag{2.49}$$

2.5 A Semi-Analytical Approximation via the HBIM to the Simplified Double-Diffusivity Heat Transfer Model

In this section we show how the double-diffusivity heat transfer model can be decoupled, producing two linear partial differential equations, which can then be solved independently using the HBIM.

Upon observing the physical values of the constants in the double-diffusivity heat transfer model (2.12), we find there exists a difference of approximately two orders of magnitude in the time scales on which T_a and T_g initially evolve. This can be explained by the fact that the thermal diffusivity of air is higher than the thermal diffusivity of grain, which results in the heat front moving faster through the air than the grain, and hence heating up faster. Grain has a lower thermal diffusivity and a higher heat storage capacity than air, which means that most of the heat is absorbed, with the rest being conducted. Hence, initially the heating is a result of heat convection, so the ratio of the diffusivities K_a and K_g determines the difference in the time scales on which T_a and T_g evolve.

We model the initial behaviour in the following way: The fact that heat is moving faster through the air path than the grain path by approximately two orders of magnitude allows us to make the idealisation that within the air path, the grain temperature is effectively still at its initial temperature, that is, $T_g = T_0$, and within the grain path, the air temperature has effectively reached the steady-state

boundary temperature, that is, $T_a = T_b$. This observation allows us to simplify, and hence decouple equation (2.12), to obtain the following two equations, which represent the change in temperature through the air and grain, respectively,

$$\frac{\partial T_a}{\partial t} = K_a \frac{\partial^2 T_a}{\partial x^2} - k_1 T_a + k_1 T_0, \tag{2.50}$$

$$\frac{\partial T_g}{\partial t} = K_g \frac{\partial^2 T_g}{\partial x^2} - k_2 T_g + k_2 T_b, \tag{2.51}$$

where T_b is a constant boundary temperature. The difference in the time scales on which T_a and T_g initially evolve is the ratio of the heat diffusivities, K_g to K_a, as initially the heating is a result of heat convection, that is,

$$\frac{K_g}{K_a} = \frac{8.3 \times 10^{-8}}{2.2 \times 10^{-5}} = 3.8 \times 10^{-3}. \tag{2.52}$$

Hence the model is accurate up until

$$t = \mathrm{O}\left(\frac{1}{3.8 \times 10^{-3}}\right) \approx 300 \text{ seconds}. \tag{2.53}$$

By applying the HBIM as detailed in the previous section to equations (2.50) and (2.51), and once again assuming penetration fronts X_a and X_g, through the air and grain respectively, along with cubic temperature profiles for both, we obtain the following explicit expressions for the temperatures of T_a and T_g, and the penetration fronts X_a and X_g, respectively,

$$T_a(x,t) = T_0 + (T_b - T_0)\left(1 - \frac{x}{X_a}\right)^3, \tag{2.54}$$

$$T_g(x,t) = T_0 + (T_b - T_0)\left(1 - \frac{x}{X_g}\right)^3, \tag{2.55}$$

$$X_a(t) = \frac{1}{k_1}\left(12k_1K_a\left\{1-\exp(-2k_1t)\right\}\right)^{1/2}, \tag{2.56}$$

$$X_g(t) = \frac{1}{k_2}\left(12k_2K_g\left\{1-\exp(-2k_2t)\right\}\right)^{1/2}, \tag{2.57}$$

Considering that for small time

$$\exp(-2k_1t) \approx 1-2k_1t \quad \text{and} \quad \exp(-2k_2t) \approx 1-2k_2t, \tag{2.58}$$

the expressions for the penetration fronts X_a and X_g, equations (2.56) and (2.57), take the forms, respectively,

$$X_a(t) = 2\sqrt{6K_a}\sqrt{t}, \tag{2.59}$$

$$X_g(t) = 2\sqrt{6K_g}\sqrt{t}, \tag{2.60}$$

which agree with the forms determined for the general double-diffusivity heat transfer model, equations (2.46) and (2.47), in the previous section.

2.6 Some Results

In this section we discuss some results pertaining to semi-analytical approximations of the simplified and general forms of the double-diffusivity heat transfer model (2.12) as developed using the HBIM. We compare these approximations to numerical approximations obtained by the explicit FTCS finite-difference scheme.

The coupled system of equations representing the penetration fronts $X_a(t)$ and $X_g(t)$ for the general double-diffusivity heat transfer model, equations (2.41) and

(2.42), were solved numerically using the Fehlberg fourth-order Runge-Kutta method as implemented in MAPLE (a symbolic algebraic computer package).

Trabelsi et al. [64] conducted a study of the dielectric properties of shelled, yellow-dent field corn, measured at different bulk densities and moisture contents. Grain temperatures ranged from 4°C to 45°C, grain moisture contents ranged from 9% to 19% wet basis and the frequencies ranged from 11GHz to 18GHz. Shelled, yellow-dent corn represents properties typical of most grains of interest to the Australian grain industry. The following is a list of the parameter values used for our examples [13, 64]: $T_b = 10\,°\mathrm{C}$, $T_0 = 0\,°\mathrm{C}$, $K_a = 2.2\,\text{E-}05\mathrm{m}^2\mathrm{s}^{-1}$, $K_g = 8.3\,\text{E-}08\mathrm{m}^2\mathrm{s}^{-1}$, $\rho_a = 1.177\,\mathrm{kgm}^{-3}$, $\rho_g = 513\,\mathrm{kgm}^{-3}$, $c_a = 1005\,\mathrm{Jkg}^{-1}{}^{\circ}\mathrm{C}^{-1}$, $c_g = 1380\,\mathrm{Jkg}^{-1}{}^{\circ}\mathrm{C}^{-1}$, $k_a = 0.01\,\mathrm{Jm}^{-3}\mathrm{s}^{-1}{}^{\circ}\mathrm{C}^{-1}$ and $\Phi_a = 0.6$, which is the fraction of grain bulk volume occupied

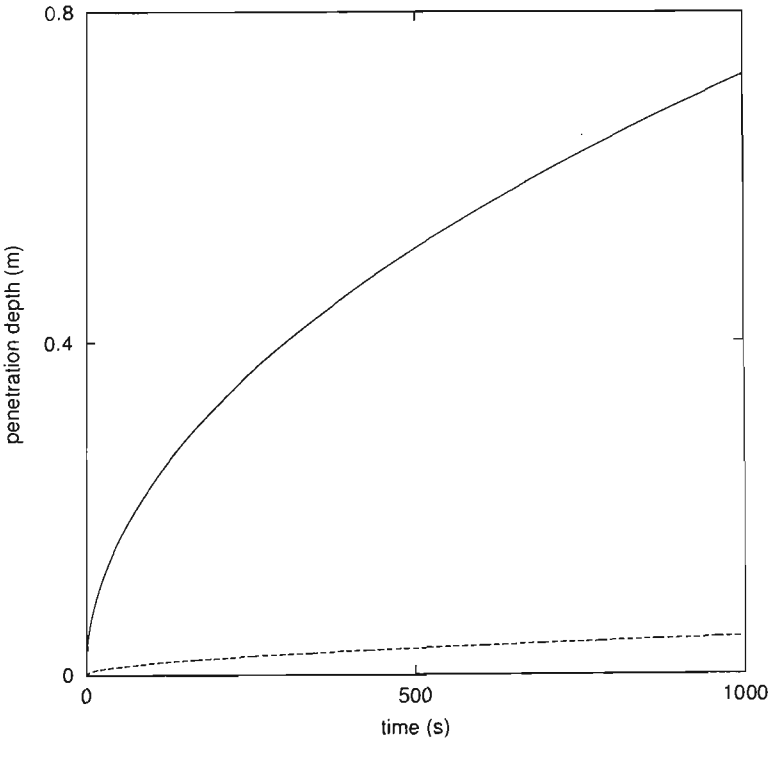

Figure 2.5: Semi-analytical approximations of the penetration depths X_a (—) and X_g (– –) versus time, up to $t = 1000$ seconds, for the simplified double-diffusivity heat transfer model.

by air. The value used for the *effective* heat transfer coefficient k_a is macroscopically averaged, and is an estimate only.

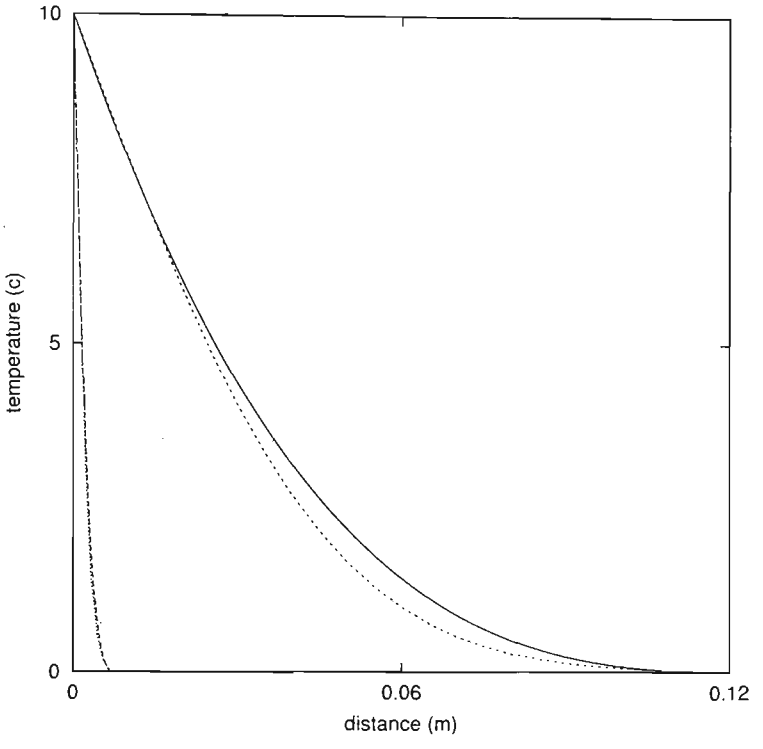

Figure 2.6: Semi-analytical and numerical approximations of the temperatures T_a, (—) and (- -), and T_g, (– –) and $(\cdots)$, respectively, versus distance, up to $t = 30$ seconds, for the simplified double-diffusivity heat transfer model.

The scenario we envisage is that of a silo wall heated by an ambient temperature of 10 °C with the air and grain at an initial temperature of 0 °C. This is typical of conditions when grain is harvested and stored in cool climates.

Figure 2.5 shows the variation of the penetrations depths $X_a(t)$ and $X_g(t)$ with time, up to $t = 1000$ seconds. Shown is the semi-analytical approximation to the simplified double-diffusivity heat transfer model, equations (2.56) and (2.57), and the numerical solution to the double-diffusivity heat transfer model (2.12). As expected, the penetration front through the air moves faster than the one through the grain, since grain has a lower thermal diffusivity than air, and a greater heat storage

capacity. We note that for early times, the profiles of the two penetration fronts are of the form $C\sqrt{t}$, as was proven in the previous section.

Figure 2.6 shows the variation of the temperatures T_a and T_g with distance, up to $t = 30$ seconds. Shown is the semi-analytical approximation to the simplified double-diffusivity heat transfer model, equations (2.54) and (2.55), and the numerical solution to the double-diffusivity heat transfer model (2.12). As a result of the heat penetrating further through the air than the grain, after the same amount of time has elapsed, we observe that there exists a noticeable difference between the air and grain temperatures. There is seen to be very good agreement between the semi-analytical and numerical solutions.

Figure 2.7 shows the variation of the temperatures T_a and T_g with time, up to

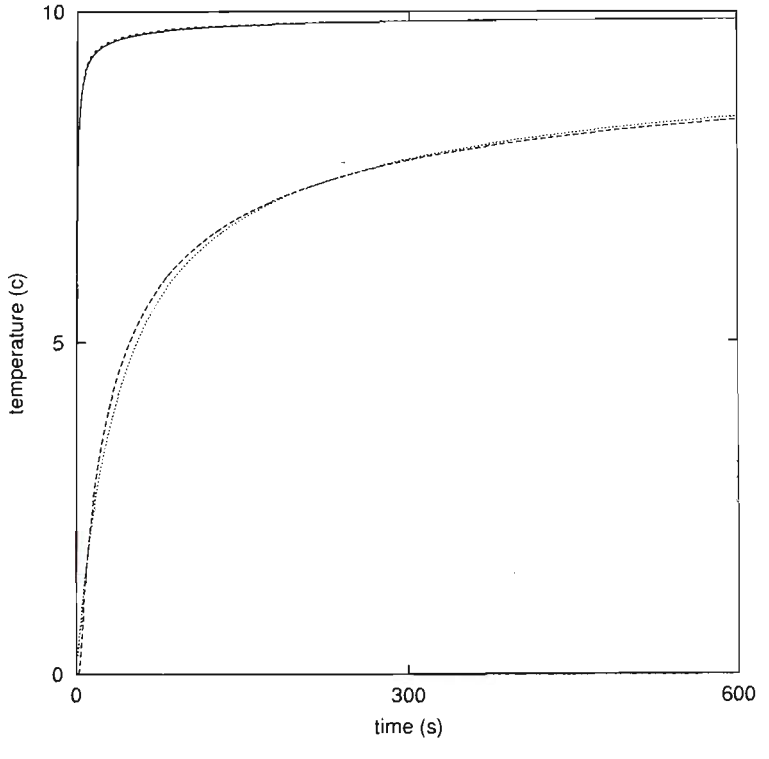

Figure 2.7: Semi-analytical and numerical approximations of the temperatures T_a, (—) and (- -), and T_g, (– –) and (· · ·), respectively, versus time, at $x = 0.002$m, for the simplified double-diffusivity heat transfer model.

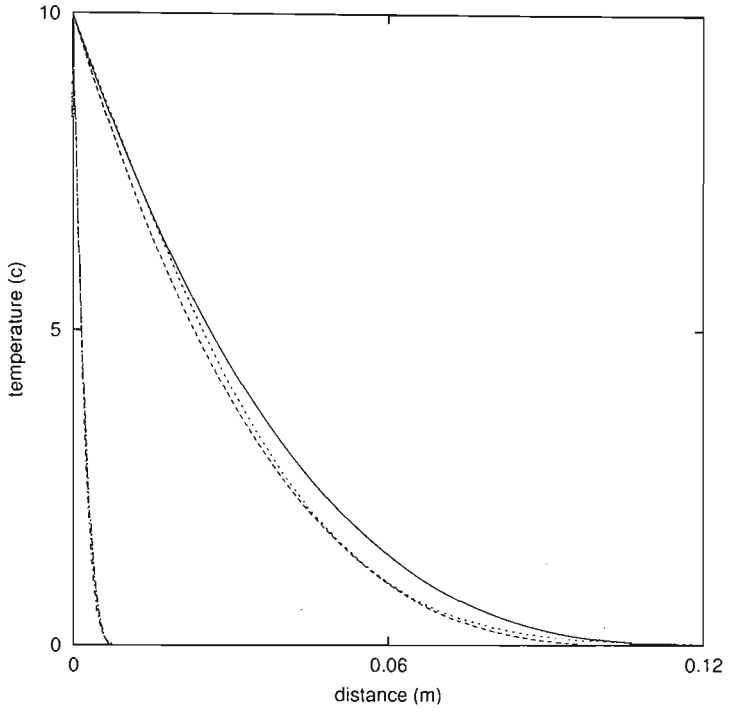

Figure 2.8: Simplified double-diffusivity heat transfer model semi-analytical, general double-diffusivity heat transfer model semi-analytical and numerical approximations of the temperatures T_a, (- -), (– –) and (—), and T_g, (· – ·), (– · ·) and (· · ·), respectively, versus distance, up to $t = 30$s.

$t = 600$ seconds, at a distance of 0.002m from the silo wall. Shown is the semi-analytical approximation to the simplified double-diffusivity heat transfer model, equations (2.54) and (2.55), and the numerical solution to the double-diffusivity heat transfer model (2.12). The figure illustrates the change in shape with time of the temperature profiles of air and grain at the point $x = 0.002$m. As time increases, the model predicts that the air and grain temperatures will reach a steady-state temperature; the boundary temperature $T_b = 10\,°\text{C}$. Furthermore, we observe that the temperature of the air approaches the steady-state temperature faster than that of the grain, as expected. Once again, there is seen to be very good agreement between the semi-analytical and numerical solutions.

Figure 2.8 shows the variation of the temperatures T_a and T_g with distance, up to $t = 30$ seconds. Shown are the semi-analytical approximations to the simplified double-diffusivity heat transfer model, equations (2.54) and (2.55), and the general double-diffusivity heat transfer model, equations (2.29) and (2.44), along with the numerical solution to the double-diffusivity heat transfer model (2.12). As expected, both models predict that the air temperature is greater than the grain temperature. We observe that the agreement between the semi-analytical approximations of the simplified and general forms is very good and that they both agree very well with the numerical solution.

2.7 Conclusions

In this chapter we have outlined the derivation of the double-diffusivity heat transfer model, and have shown how this formulation is based on the double-diffusivity model. We have developed semi-analytical approximations to both the simplified and general forms of the double-diffusivity heat transfer model, by using the HBIM. We have also compared these approximations to numerical approximations, and the results have shown that the two approximations agree very well, for both the simplified and general forms of the model. The agreement between the simplified and general forms of the double-diffusivity heat transfer model was also shown to be very good. These approximations illustrate that the double-diffusivity heat transfer model predicts that there exists a noticeable difference between the air and grain temperatures of a grain bulk, with the penetration of heat moving faster through the

air than the grain, which is fundamentally based on the difference in their thermal diffusivity values, particularly for early time, which is of primary interest to us. The approximations also show that for early times the penetration fronts take the form $C\sqrt{t}$.

Chapter 3

The Two-Stage Heat Transfer Model

3.1 Introduction

In this chapter we derive the two-stage heat transfer model, which is based on a heat transfer variant of the two-stage model originally proposed by McNabb [40]. We discuss why such a model is used, and obtain a semi-analytical approximation via Laplace transforms valid for small and large times. These semi-analytical approximations are compared with numerical approximations obtained using the Stehfest [58] algorithm. We also compare this model to the double-diffusivity heat transfer model derived in the previous chapter.

3.2 Mathematical Formulation

We begin by outlining the development of McNabb's [40] two-stage model, and then illustrate the derivation of the two-stage heat transfer model.

3.2.1 Derivation of The Two-Stage Model

McNabb [40] proposed a two-stage model for the modelling of the propagation of pressures in a porous medium with its permeability affected by a homogeneous distribution of fissures, which effectively partitions the medium into blocks of a particular geometry. This results in two pressures that are associated with the medium, one with the fissures, and the other with the blocks.

McNabb observed that in order to model such systems in their most general form, the problem of dimensionality must be considered. Three variables are needed to first locate the block within the system, and then another four variables, three of space and one of time, are required to describe the block itself. For certain cases of these problems, a factorisation can be used such that the two systems, the fissures and the blocks, can be essentially uncoupled. This then lends itself to a method of solution via Laplace transforms.

The two-stage model is based on the assumption that in the neighbourhood of every point x in the fissure system, there is associated a block, and within each block there is associated a specific geometry with a different spatial coordinate system y. Hence, the model is composed of two diffusion equations, one for the pressure change in the fissures, and one for the pressure change in the blocks. These two

diffusion equations are coupled together by the changes in fissure pressure acting as a boundary condition for the blocks located in its neighbourhood.

It is assumed that the fissure permeability is high enough compared to the block permeability so that the pressure drop in the fissure system across a typical block is negligible. It is also assumed that the fissure system is in contact with the block system everywhere, that is, it is continuous, with pressure changes only reaching the blocks via the fissure systems, and hence the blocks act as a distribution source of fluids to the fissure system. The corresponding equations are

$$\begin{aligned}
\Phi_f \mu c \frac{\partial P_f}{\partial t} &= K_f \frac{\partial^2 P_f}{\partial x^2} + F(x,t), \\
\Phi_b \mu c \frac{\partial P_b}{\partial t} &= K_b \frac{\partial^2 P_b}{\partial y^2}, \qquad y \in V_x, \\
F(x,t) &= \frac{K_b}{V_x} \int\int_{S_x} \frac{\partial P_b}{\partial y} \cdot d\sigma, \quad y \in S_x, \\
P_b(x,y,t) &= P_f(x,t), \qquad y \in S_x,
\end{aligned} \tag{3.1}$$

where P_f is the fluid pressure in the fissure system at position x at time t, P_b is the pressure change in the block at position y at time t located in the neighbourhood of position x, Φ_f is the porosity of the fissure system, Φ_b is the porosity of the blocks, μ is the dynamic viscosity of the fluid, c is the compressibility of the fluid at constant pressure, K_f is the permeability of the fissure system, K_b is the permeability of the blocks, V_x is the volume of block in the neighbourhood of position x and S_x is the surface of the block in the neighbourhood of position x.

This model is sometimes referred to as the *Fruitcake Model*, since it is analogous

to modelling diffusion in a fruitcake consisting of a cake mix (or highly permeable fissures) and fruit (less permeable blocks).

3.2.2 Derivation of The Two-Stage Heat Transfer Model

To adopt the McNabb approach for our grain store heat transfer problem, we begin by making the assumption that the grains are all uniform in size and spherical in shape. This is a legitimate assumption to make, in particular, for the case of canola, which is a grain that is currently of great interest to the Australian grain industry.

The model distinguishes between the air and grain whereby heat flows through the air to the grain, and is transferred into the grain through its surface. The actual grain geometry is taken into consideration using a separate spatial coordinate system, in order to represent the temperature at various points within each grain kernel. Hence, there are two separate spatial coordinate systems used, one for the grain bulk (macroscopic) and one for the grain kernel (microscopic), as illustrated in Figure 3.1.

The heat transfer within the peripheral layer is most critical when internal convection cells are not fully established. Convective currents are thus assumed to be negligible, allowing analysis of such situations. Thus, analogously to McNabb's

two-stage model, the one-dimensional two-stage heat transfer model is:

$$\begin{aligned}
\frac{\partial T_a}{\partial t} &= K_a \frac{\partial^2 T_a}{\partial x^2} - \frac{F(x,t)}{\rho_a c_a}, \\
\frac{\partial T_g}{\partial t} &= K_g \left(\frac{\partial^2 T_g}{\partial r^2} + \frac{2}{r} \frac{\partial T_g}{\partial r} \right), \\
F(x,t) &= \frac{3\kappa_g (1 - \Phi_a)}{a} \frac{\partial T_g}{\partial r}, \\
T_g(x,a,t) &= T_a(x,t),
\end{aligned} \tag{3.2}$$

with the following initial conditions and boundary conditions:

$$T_a(x,0) = T_0, \quad T_g(x,r,0) = T_0 \quad \text{and} \quad T_a(0,t) = T_b, \tag{3.3}$$

and where T_a is the temperature of the air, T_g is the temperature of the grain, K_a is the thermal diffusivity of the air, K_g is the thermal diffusivity of the grain, r is the spatial coordinate system in the grain kernel, a is the radius of the grain kernel and Φ_a is the fraction of grain bulk volume occupied by air.

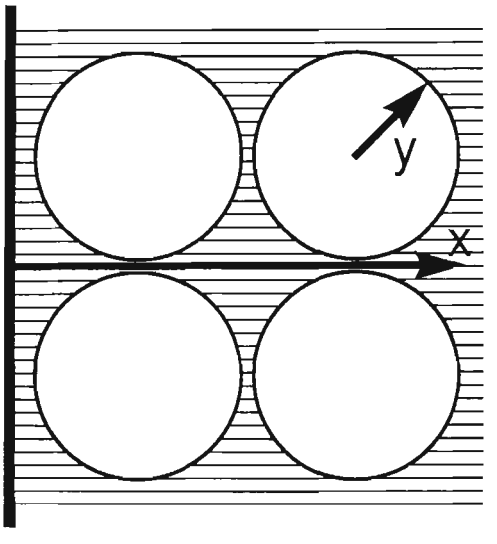

Figure 3.1: Idealisation of the two-stage heat transfer model.

Equation $(3.2)_1$ describes the temperature of the air, including a sink term F. Equation $(3.2)_2$ describes the internal temperature of the grain. Equation $(3.2)_3$ is the sink term, describing the transfer of heat from air to grain through the surface of the grain, and equation $(3.2)_4$ is the continuity boundary condition, which states that on the surface of the grain, the air and grain temperatures are equal.

3.3 Semi-Analytical Approximations via Laplace Transforms

As mentioned previously, the two-stage heat transfer model lends itself to a solution technique involving Laplace transforms. We obtain a semi-analytical approximation via Laplace transforms, whereby small and large time inversions of the Laplace transforms are compared with numerical inversions obtained using the Stehfest [58] algorithm.

The solution technique is as follows:

1. We begin by first solving equation $(3.2)_2$ for $T_g(x, r, t)$ using equation $(3.2)_4$ as the boundary condition.

2. We then calculate equation $(3.2)_3$ from the previously determined value of $T_g(x, r, t)$, which gives an expression for the sink term $F(x, t)$.

3. We then substitute this into equation $(3.2)_1$, and finally solve for $T_a(x, t)$.

The solution is thus a two-stage one, as we first solve the equations governing the microstructure of the grain bulk, which are linked to the surrounding air via the

continuity boundary conditions, this then allows us to solve the equations governing the macrostructure, that is, the air.

To begin, we take Laplace transforms with respect to time, and follow this with a factorisation approach in Laplace transform space, which allows us to separate into functions of both (x, s) and (r, s). Upon taking Laplace transforms with respect to time of equation (3.2), and assuming zero initial conditions, we have

$$\begin{aligned}
\frac{\partial^2 \overline{T}_a}{\partial x^2} &= \frac{1}{K_a}\left(s\overline{T}_a + \frac{\overline{F}(x,s)}{\rho_a c_a}\right), \\
\frac{1}{r^2}\frac{\partial}{\partial r}\left(r^2 \frac{\partial \overline{T}_g}{\partial r}\right) &= \frac{s}{K_g}\overline{T}_g, \\
\overline{F}(x,s) &= \frac{3\kappa_g(1-\Phi_a)}{a}\frac{\partial \overline{T}_g}{\partial r}(x,a,s), \\
\overline{T}_g(x,a,s) &= \overline{T}_a(x,s),
\end{aligned} \tag{3.4}$$

We now assume a factorisation. The physical significance of this factorisation means that the structure of the grain is independent of its position within the grain bulk, while the mathematical significance allows us to perform a separation of variables, specifically, into functions of x and r. The factorisation is as follows

$$\overline{T}_g(x,r,s) = \overline{T}_a(x,s)\,\Omega(r,s), \tag{3.5}$$

where $\Omega(r,s)$ is such that

$$\begin{aligned} \frac{1}{r^2}\frac{\partial}{\partial r}\left(r^2\frac{\partial\Omega}{\partial r}\right) &= \frac{s}{K_g}\Omega, \quad r<a, \\ \Omega &= 1, \qquad r=a, \\ \lim_{r\to 0}\left(r^2\frac{\partial\Omega}{\partial r}\right) &= 0. \end{aligned} \tag{3.6}$$

The solution to equation $(3.6)_1$ can easily be found to be

$$\Omega(r,s) = \frac{\sinh\left(r\sqrt{s/K_g}\right)a}{\sinh\left(a\sqrt{s/K_g}\right)r}. \tag{3.7}$$

Using equations (3.5) and (3.7), equation $(3.4)_3$ becomes

$$\overline{F}(x,s) = \frac{3\kappa_g(1-\Phi_a)}{a}\overline{T}_a(x,s)\frac{\partial\Omega}{\partial r}(a,s). \tag{3.8}$$

Now,

$$\frac{\partial\Omega}{\partial r}(a,s) = \sqrt{\frac{s}{K_g}}\coth\left(a\sqrt{s/K_g}\right) - \frac{1}{a}. \tag{3.9}$$

Thus, we have the following expression for the sink term

$$\overline{F}(x,s) = \frac{3\kappa_g(1-\Phi_a)}{a}\overline{T}_a(x,s)\left\{\sqrt{\frac{s}{K_g}}\coth\left(a\sqrt{s/K_g}\right) - \frac{1}{a}\right\}. \tag{3.10}$$

Therefore, equation $(3.4)_1$ becomes

$$\frac{\partial^2\overline{T}_a}{\partial x^2} = \overline{T}_a\left\{\frac{1}{K_a}\left(s + \frac{3\kappa_g(1-\Phi_a)}{a\rho_a c_a}\left\{\sqrt{\frac{s}{K_g}}\coth\left(a\sqrt{s/K_g}\right) - \frac{1}{a}\right\}\right)\right\}. \tag{3.11}$$

Using the transformed boundary conditions,

$$\overline{T}_a(0,s) = \frac{T_b}{s} \quad \text{and} \quad \lim_{x\to\infty}\overline{T}_a(x,s) = 0, \tag{3.12}$$

we can easily find the solution to equation (3.11),

$$\overline{T}_a(x,s) = \frac{T_b}{s} e^{-x\sqrt{p}}, \tag{3.13}$$

where

$$p = \frac{1}{K_a}\left(s + \frac{3\kappa_g(1-\Phi_a)}{a\rho_a c_a}\left\{\sqrt{\frac{s}{K_g}}\coth\left(a\sqrt{s/K_g}\right) - \frac{1}{a}\right\}\right). \tag{3.14}$$

From equation (3.5), we obtain

$$\overline{T}_g(x,r,s) = \frac{T_b}{s} e^{-x\sqrt{p}} \frac{\sinh\left(r\sqrt{s/K_g}\right) a}{\sinh\left(a\sqrt{s/K_g}\right) r}. \tag{3.15}$$

Since it is not possible to obtain inverse Laplace transforms of equations (3.13) and (3.15) analytically, we obtain semi-analytical solutions by considering inversions of small and large time approximations.

3.3.1 A Semi-Analytical Small Time Approximation

In this section we obtain inversions of equations (3.13) and (3.15), by considering small time approximations, which corresponds to the limit as $s \to \infty$.

We will first determine an expression for $\overline{T}_a(x,s)$. We begin by considering the limit as $s \to \infty$ for p. Using $\lim_{s\to\infty} \coth(s) = 1$, we obtain

$$\lim_{s\to\infty} p = \frac{1}{K_a}\left(s + \frac{3\kappa_g(1-\Phi_a)}{a\rho_a c_a}\left\{\sqrt{\frac{s}{K_g}} - \frac{1}{a}\right\}\right). \tag{3.16}$$

Hence,

$$\lim_{s\to\infty} p = \frac{1}{K_a}\left(s + m_1\sqrt{s} - m_2\right), \tag{3.17}$$

where

$$m_1 = \frac{3\kappa_g(1-\Phi_a)}{a\rho_a c_a\sqrt{K_g}} \quad \text{and} \quad m_2 = \frac{3\kappa_g(1-\Phi_a)}{a^2\rho_a c_a}. \tag{3.18}$$

Now,

$$\begin{aligned}(s+m_1\sqrt{s}-m_2)^{1/2} &= s^{1/2}\left(1+\left\{\frac{m_1}{\sqrt{s}}-\frac{m_2}{s}\right\}\right)^{1/2}, \\ &\approx s^{1/2}+\frac{m_1}{2}.\end{aligned} \tag{3.19}$$

We hence obtain the following expression for $\overline{T}_a(x,s)$:

$$\lim_{s\to\infty}\overline{T}_a(x,s) = \frac{T_b}{s}\exp\left\{\frac{-xm_1}{2\sqrt{K_a}}\right\}\exp\left\{\frac{-x}{\sqrt{K_a}}s^{1/2}\right\}. \tag{3.20}$$

We will now determine a small time approximation to $\overline{T}_g(x,s)$. Consider

$$\lim_{s\to\infty}\frac{\sinh\left(r\sqrt{s/K_g}\right)a}{\sinh\left(a\sqrt{s/K_g}\right)r} = \frac{a}{r}\exp\left\{(r-a)\sqrt{s/K_g}\right\}. \tag{3.21}$$

From equations (3.15) and (3.20), we obtain the following expression for $\overline{T}_g(x,s)$:

$$\lim_{s\to\infty}\overline{T}_g(a,r,s) = \frac{aT_b}{rs}\exp\left\{\frac{-xm_1}{2\sqrt{K_a}}\right\}\exp\left\{\left(\frac{(r-a)}{\sqrt{K_g}}-\frac{x}{\sqrt{K_a}}\right)\sqrt{s}\right\}. \tag{3.22}$$

Upon inverting using MAPLE, the small time expressions for $T_a(x,s)$ and $T_g(x,s)$, respectively, are:

$$\lim_{t\to 0}T_a(x,t) = T_b\exp\left\{\frac{-3x\kappa_g(1-\Phi_a)}{2a\rho_a c_a\sqrt{K_a}\sqrt{K_g}}\right\}\operatorname{erfc}\left\{\frac{x}{2\sqrt{K_a}\sqrt{t}}\right\}, \tag{3.23}$$

and

$$\begin{aligned}\lim_{t\to 0}T_g(x,r,t) &= \\ &\frac{aT_b}{r}\exp\left\{\frac{-3x\kappa_g(1-\Phi_a)}{2a\rho_a c_a\sqrt{K_a}\sqrt{K_g}}\right\}\operatorname{erfc}\left\{\frac{-1}{2\sqrt{t}}\left(\frac{(r-a)}{\sqrt{K_g}}-\frac{x}{\sqrt{K_a}}\right)\right\},\end{aligned} \tag{3.24}$$

where erfc is the usual complementary error function.

3.3.2 A Semi-Analytical Large Time Approximation

In this section we obtain inversions of equations (3.13) and (3.15), by considering large time approximations, which corresponds to the limit as $s \to 0$.

We begin by determining a large time approximation to T_a. If we consider the fact that for small y, we have the approximation $\coth(y) = 1/y + y/3 + \mathrm{O}(y^3)$, we obtain

$$\lim_{s\to 0} p = \frac{1}{K_a}\left\{s + \left(1 + \frac{\kappa_g(1-\Phi_a)}{K_g\rho_a c_a}\right)\right\}. \tag{3.25}$$

Thus, the expression for $\overline{T}_a(x,s)$ becomes

$$\lim_{s\to 0}\overline{T}_a(x,s) = \frac{T_b}{s}\exp\left\{-xs^{1/2}\left\{\frac{1}{K_a}\left(1 + \frac{\kappa_g(1-\Phi_a)}{K_g\rho_a c_a}\right)\right\}^{1/2}\right\}. \tag{3.26}$$

We will now determine a large time approximation to T_g. Consider

$$\lim_{s\to 0}\frac{\sinh\left(r\sqrt{s/K_g}\right)a}{\sinh\left(a\sqrt{s/K_g}\right)r} = \frac{a\left(e^{r\sqrt{s/K_g}} - e^{-r\sqrt{s/K_g}}\right)}{r\left(e^{a\sqrt{s/K_g}} - e^{-a\sqrt{s/K_g}}\right)}, \tag{3.27}$$

and so by using L'Hopitals rule, we find

$$\lim_{s\to 0}\frac{a(r/K_g)1/2s^{-1/2}\cosh\left(r\sqrt{s/K_g}\right)}{r(a/K_g)1/2s^{-1/2}\cosh\left(a\sqrt{s/K_g}\right)} = 1. \tag{3.28}$$

Thus, from equations (3.15) and (3.26), we obtain

$$\lim_{s\to 0}\overline{T}_g(a,r,s) = \lim_{s\to 0}\overline{T}_a(x,s). \tag{3.29}$$

Upon inverting via MAPLE, we have the following large time approximations to $T_a(x,s)$ and $T_g(x,s)$:

$$\begin{aligned}\lim_{t\to\infty} T_a(x,t) &= T_b\,\mathrm{erfc}\left\{\frac{x}{2\sqrt{t}}\left(\frac{1}{K_a}\left\{1 + \frac{\kappa_g(1-\Phi_a)}{\rho_a c_a K_g}\right\}\right)^{1/2}\right\}. \\ &= \lim_{t\to\infty} T_g(x,r,t),\end{aligned} \tag{3.30}$$

We observe that for large times, the air and grain temperatures are equal to one another, due to the fact that equilibrium is reached (steady-state temperature), that is, $T_a = T_g = T_b$ in the limit $t \to \infty$.

3.4 Some Results

In this section we discuss some results pertaining to semi-analytical and numerical approximations of the two-stage heat transfer model. The numerical approximations have been developed using the Stehfest [58] algorithm, a well known algorithm for diffusion problems, to obtain numerical inverse Laplace transforms of equations (3.13) and (3.15).

The same parameter values are used as those in Chapter 2, and the same grain heating scenario is envisaged. We have used a macroscopically averaged value for the thermal conductivity of grain, $\kappa_g = 0.001\,\mathrm{Jm^{-1}s^{-1}{}^{\circ}C^{-1}}$, and it is an estimate only. Note that the temperature of the grain is measured near the centre of the grain kernel ($r = 0.001\,\mathrm{m}$), where the radius is taken to be $a = 0.005\,\mathrm{m}$.

In the implementation of the Stehfest [58] algorithm, we used an N_p value of 18. N_p is known as the *Stehfest parameter*. It is the number of terms to be summed in one part of the Stehfest [58] algorithm. In principle, the larger the value of N_p, the more accurate the numerical inversion. In practice, though, the choice of N_p is limited by truncation errors. Typical values for N_p are 10 and 18. For $N_p = 10$, the inversions are accurate up to 8 decimal places, while for $N_p = 18$, the accuracy is approximately double that.

The semi-analytical approximations presented pertain to small time approximations. Results pertaining to large time approximations are not illustrated, as it was proven analytically in the previous section that the air and grain temperatures are equal. Comparisons of the semi-analytical and numerical approximations for small

and large times are not illustrated as the semi-analytical and numerical approximations are the same, to graphical accuracy. Instead, results are illustrated for moderate times.

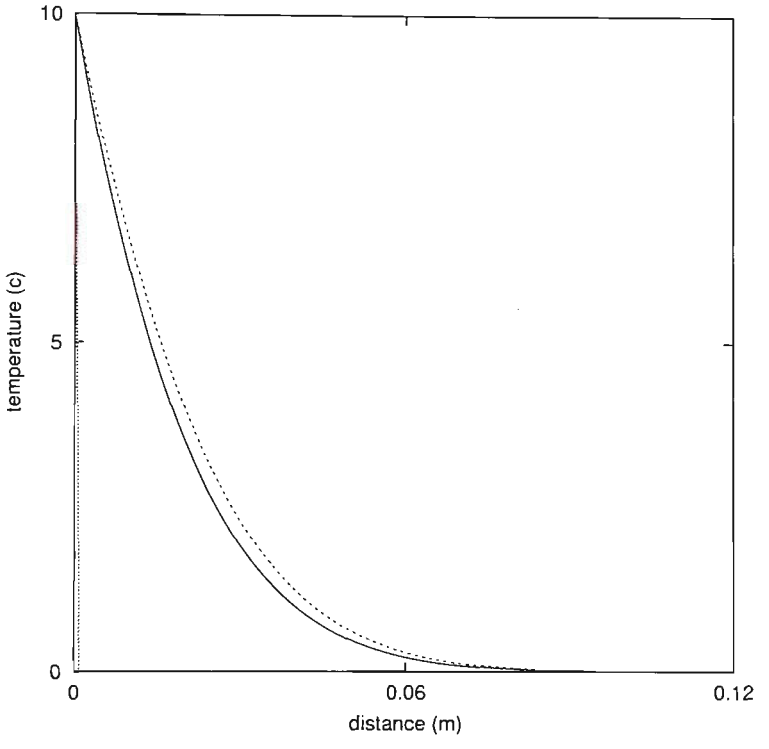

Figure 3.2: Semi-analytical and numerical approximations of the temperatures T_a, (—) and (- -), and T_g, (– –) and $(\cdots)$, versus distance, up to $t = 30$ seconds.

Figure 3.2 shows the variation of the temperatures T_a and T_g with distance, up to $t = 30$ seconds. Shown are the semi-analytical and numerical approximations to the two-stage heat transfer model, equations (3.23) and (3.24), and equations (3.13) and (3.15). We observe that there is a difference between the air and grain profiles, with the heat penetrating noticeably further through the air than the grain after the same amount of time has elapsed. Good agreement is observed between the semi-analytical and numerical solutions. The semi-analytical grain temperature, T_g (– –), is not noticeable on the figure as there is effectively no penetration through

the grain after such a short time, however, we observe from Figure 3.3 that the grain temperature rises above 0°C after approximately 80 seconds.

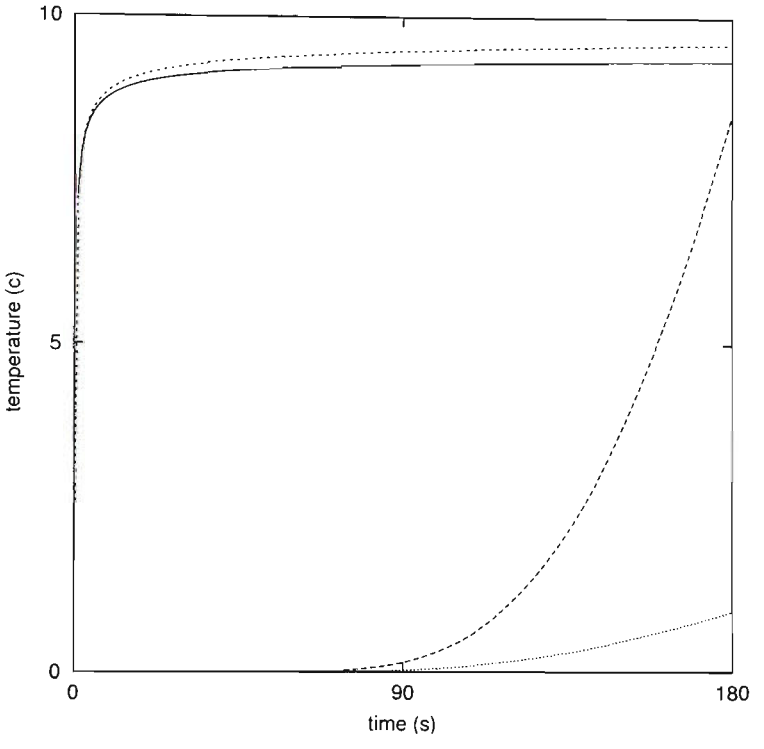

Figure 3.3: Semi-analytical and numerical approximations of the temperatures T_a, (—) and (- -), and T_g, (– –) and $(\cdots)$, versus time, at $x = 0.002$m.

Figure 3.3 shows the variation of the temperatures T_a and T_g with time, up to 180 seconds, at a distance of 0.002m from the silo wall. Shown are the semi-analytical and numerical approximations to the two-stage heat transfer model, equations (3.23) and (3.24), and equations (3.13) and (3.15). The figure illustrates the change in shape with time of the temperature profiles of air and grain, at the point $x = 0.002$m. Due to the difference in the time scale evolutions of the two profiles, the temperature of the air approaches the steady-state temperature $T_b = 10\,°\text{C}$ faster, as expected. Furthermore, due to the fact that the two temperatures are modelled differently, their profiles appear different in shape. Additionally, the figure shows that as time

tends to infinity, both the air and grain temperatures approach the steady-state temperature $T_b = 10\,^{\circ}\mathrm{C}$. This is clearly seen in Figure 3.5, where a larger time scale is considered. Good agreement is observed between the semi-analytical and numerical solutions, particularly for the air temperature approximations. We observe that as time increases, the agreement between the small time semi-analytical solution and the numerical solution decreases, which is to be expected.

3.5 Comparison of the Double-Diffusivity Heat Transfer and the Two-Stage Heat Transfer Models

In this section we examine the differences between the double-diffusivity heat transfer and the two-stage heat transfer models. We begin by discussing their theoretical fundamental differences, and then perform a qualitative comparison using some results.

3.5.1 Theoretical Comparisons

Both the double-diffusivity heat transfer model and the two-stage heat transfer model are *dual-region* models in that they identify air and grain temperatures separately within the grain bulk. The microscopic configuration of the grain bulk is important to both models in order to obtain a well-defined macroscopic description. The two models differ in how they identify this microstructure, however.

The fundamental assumption behind the double-diffusivity model is that there exist two connection pathways, such that each point within the grain bulk is occupied by both air and grain, hence the temperature at that point is the average or weighted average of the two temperatures. Heat transfer takes place along either the air or the grain path, with the possibility of heat being transferred from one path to the other.

The main criticism of such an approach, such as discussed in Streltsova-Adams [59], in reference to Barenblatt's [10] double-porosity model, is the assumption that any infinitesimally small volume of the grain bulk is occupied by *both* air and grain, meaning that it is impossible to know whether a particular point lies within either the air *or* the grain. The two-stage heat transfer model does not suffer such a drawback. It also considers a double-porosity mechanism, but takes into consideration the distribution of the grain through the air, and uses a greater level of detail for the temperature of the grain particles. The double-diffusivity heat transfer model treats the grain particle as a *lump* with one uniform temperature, whereas the two-stage heat transfer model identifies a separate spatial coordinate system within the grain, that is, it considers the variation in temperature with distance from the centre of the grain kernel.

The two-stage approach requires the identification of a characteristic length scale associated with the microstructure of the medium, which can, in general, prove to be quite difficult. The double-diffusivity approach, however, does not require such an identification, since it assumes a random microstructure throughout the medium, effectively not requiring the association of a characteristic length scale. The problem,

however, lies in identifying the values of the *effective* heat transfer coefficients of air and grain across some area. These are very difficult to determine for a medium, such as a grain bulk, that assumes that each point is occupied by both air and grain.

The double-diffusivity heat transfer model effectively considers two overlapping paths for heat conduction, notably, the air and grain paths. Each path fills the entire grain bulk, such that at every point within the grain bulk there may be a change of path. Consequently, the variables and coefficients of the model are macroscopically averaged values at a point. The two-stage heat transfer model considers the grain bulk to be composed of two separate regions within which heat transfer may occur, with an interaction occurring between the two across a boundary interface.

In summary, the main difference between the two models is the level of detail concerning the temperature of the air and grain particles, in particular, the grain particles. The double-diffusivity heat transfer model treats the grain as one *lump* and as such there exists one grain temperature only, whereas the two-stage heat transfer model considers the variation of temperature from the centre of the grain particle.

3.5.2 Comparison by Some Results

In this section we discuss some results pertaining to the numerical approximation of the simplified double-diffusivity heat transfer model, and the numerical approximation of the two-stage heat transfer model.

We can only perform a qualitative comparison of the two models, since they are fundamentally different to one another. This is primarily due to the fact that the

two-stage heat transfer model predicts the temperature at various points within the grain, whereas the double-diffusivity heat transfer model predicts one bulk grain temperature.

The same parameter values are used as in the previous section, and the same scenario is considered.

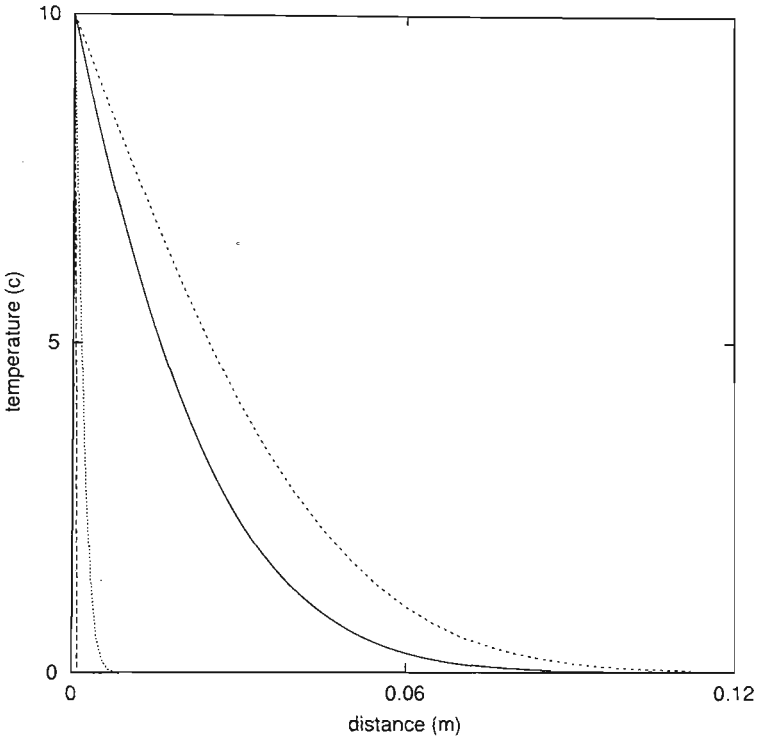

Figure 3.4: Two-stage and double-diffusivity numerical approximations of the temperatures T_a, (—) and (- -), and T_g, (– –) and $(\cdots)$, respectively, versus distance, up to $t = 30$ seconds.

Figure 3.4 shows the variation of the temperatures T_a and T_g with distance, up to $t = 30$ seconds. Shown are the numerical approximations to the two-stage and double-diffusivity heat transfer models. We observe that both the air and grain temperatures of the two-stage heat transfer model lag behind those of the double-diffusivity heat transfer model. In other words, after the same amount of time has elapsed, the predictions for the air and grain temperatures of the double-diffusivity

heat transfer model are greater than those of the two-stage heat transfer model. This is due to the fundamental difference in the way in which the two models define the air and grain temperatures. Both models predict that there exists a difference in the air and grain temperatures, with the air temperature being greater than the grain temperature. In Figure 3.5 we observe that this difference decreases as time increases.

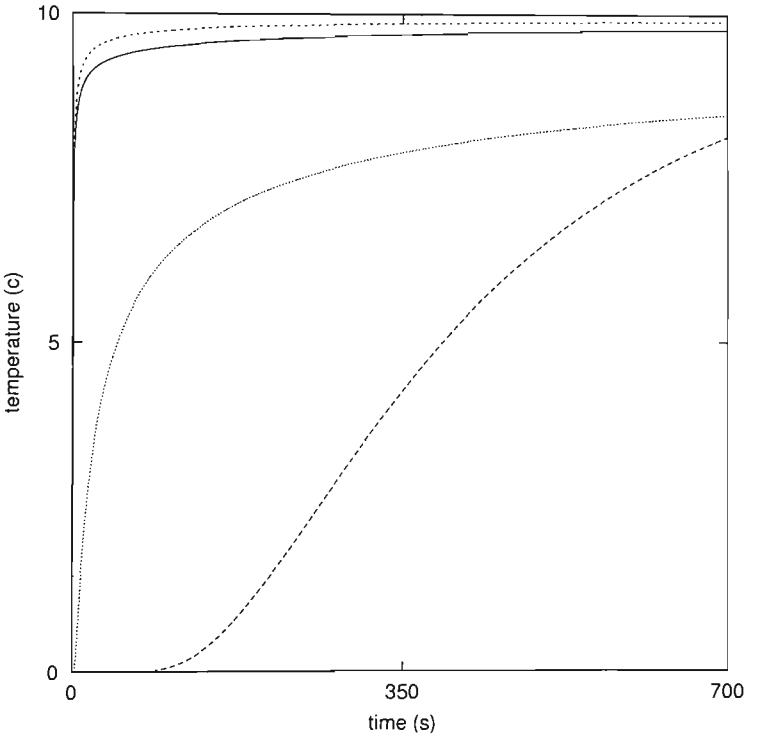

Figure 3.5: Two-stage and double-diffusivity numerical approximations of the temperatures T_a, (—) and (- -), and T_g, (– –) and $(\cdots)$, respectively, versus time, at $x = 0.002$m.

Figure 3.5 shows the variation of the temperatures T_a and T_g with time, up to $t = 700$ seconds, at a distance of 0.002m from the silo wall. Shown are the numerical approximations to the two-stage and double-diffusivity heat transfer models. Once again, we observe that both the air and grain temperatures of the two-stage model lag behind those of the double-diffusivity heat transfer model, which approach the

steady-state temperature $T_b = 10\,^{\circ}\mathrm{C}$ faster. We also note that the profile of the grain temperature prediction for the two-stage heat transfer model is different to that of the double-diffusivity heat transfer model. This is primarily due to the fundamental difference in how the two models define the grain temperature. Both models predict that as time tends to infinity, the air and grain temperatures reach a steady-state temperature $T_b = 10\,^{\circ}\mathrm{C}$.

3.6 Conclusions

In this chapter we have outlined the derivation of the two-stage heat transfer model, and have shown how this formulation is based on the two-stage model, as proposed by McNabb [40].

We have developed a semi-analytical approximation using Laplace transforms, whereby small and large time semi-analytical inversions of the Laplace transforms have been compared to numerical inversions obtained using the Stehfest [58] algorithm. The results presented illustrate that the two solutions agree very well with one another for small time, while good agreement is noted for moderate time as well.

We have also outlined the theoretical fundamental differences between the double-diffusivity heat transfer and the two-stage heat transfer models, and have discussed some of the main qualitative differences of the two models by way of some results. Both models predict that there exists a difference in the air and grain temperatures of the grain bulk, with both predicting that the heat penetrates faster through the air than the grain, as one would expect. We observe that the air and grain tempera-

tures of the two-stage heat transfer model lag behind those of the double-diffusivity heat transfer model, with the lag decreasing as time increases. This is related to the fundamental differences that exist between the two models, in particular, pertaining to the way in which the models define, not only the microstructure of the air and grain, but the interaction that exists between air and grain.

We note that for the simplified form of the double-diffusivity heat transfer model we are able to determine exact analytical expressions for the air and grain temperatures, equations (2.54) and (2.55), whereas for the two-stage heat transfer model we can only obtain small and large time analytical approximations, equations (3.23) and (3.24) and equation (3.30). Furthermore, the numerical approximation to the two-stage heat transfer model is computationally less intensive than that of the double-diffusivity heat transfer model.

Chapter 4

The Double-Diffusivity Heat Transfer Model Incorporating Microwave Heating

4.1 Introduction

In this chapter we develop the double-diffusivity heat transfer model incorporating microwave heating, which is based on the double-diffusivity heat transfer model derived previously. We illustrate how to obtain a semi-analytical approximation to this model using the HBIM. This approximation is compared to a numerical approximations obtained via an explicit finite-difference scheme.

4.2 Mathematical Formulation

We propose to model the microwave heating processes of a grain bulk by considering the general double-diffusivity heat transfer model, equation (2.12), developed in Chapter 2, with an appended body heating source term to account for heating due to microwave radiation.

The overall idea stems from the fact that, in general, it is very complicated to model microwave heating processes mathematically, as this requires the simultaneous solution of Maxwell's equations of electromagnetism, (4.1), coupled with the heat equation, in which all electrical, magnetic, and thermal properties are non-linearly dependent on the temperature of the medium being heated. The solution to such a complex coupled system of non-linear equations can be very difficult to obtain, either analytically or numerically, even if sufficient data exists for the various electrical and magnetic properties. The approach we take is similar to work done by Hill and Jennings [28], among others, and involves the addition of a body heating source term to the heat transfer model, in order to account for heat due to microwave radiation. In order to identify the body heating source term, we fitted curves to experimental data, in particular, we fit a curve of best fit to results based on yellow-dent field corn as given in Trabelsi et al. [64].

Maxwell's equations for electromagnetism [49]:

$$\begin{aligned} \triangle \cdot \mathbf{D} &= \rho_f, \qquad \triangle \times \mathbf{E} = -\frac{\partial \mathbf{B}}{\partial t}, \\ \triangle \cdot \mathbf{B} &= 0, \qquad \triangle \times \mathbf{H} = \mathbf{j_f} + \frac{\partial \mathbf{D}}{\partial t}, \end{aligned} \tag{4.1}$$

where $\mathbf{E}$ is the electric field, $\mathbf{D} = \epsilon^{'}(T)\mathbf{E}$ is the electric field displacement vector, $\mathbf{H}$

is the magnetic field, $\mathbf{B} = \mu(T)\mathbf{H}$ is the magnetic flux density, ρ_f is the free charge density, $\mathbf{j_f}$ is the free current density, $\epsilon^{'}(T) = \epsilon_r\epsilon_0$ is the electrical permittivity and $\mu(T) = \mu_r\mu_0$ is the magnetic permeability.

We begin by showing how we can use a body heating source term to model the heating due to microwave radiation. We then formulate the double-diffusivity heat transfer model with microwave heating, and then determine a semi-analytical solution using the HBIM.

4.2.1 The Body Heating Source Term

In order to obtain the form of the body heating source term, we need to calculate the amount of energy that is converted into heat as microwaves pass through the material. To do this, we must calculate the power density that is absorbed by the material.

Of all the various electrical properties of a material, the electrical conductivity $\sigma(T)$ has the most significant effect on how the material is heated. For the purpose of this work, we shall incorporate the electrical conductivity $\sigma(T)$ into the electrical permittivity $\epsilon(T)$, which will then become a complex quantity

$$\epsilon = \epsilon^{'} - i\epsilon^{''}. \tag{4.2}$$

The loss factor ($\epsilon^{''}$) is of primary interest to us, and we are particularly interested in its variation with temperature, as this is the variable in the body heating source term $Q(T)$, equation (4.6).

We begin by calculating the net power that is dissipated. To do this, we integrate

the Poynting vector over the surface of the object being heated, thus

$$P = \int_s (\mathbf{E} \times \mathbf{H}^*) \cdot d\mathbf{S}. \tag{4.3}$$

Assuming sinusoidally varying $\mathbf{B}$ and $\mathbf{D}$ fields, Metaxis and Meredith [41] showed that the average power, defined by

$$P_{\text{ave}} = -\frac{1}{2} \int_s \text{Real}(\mathbf{E} \times \mathbf{H}^*) \cdot d\mathbf{S}, \tag{4.4}$$

becomes

$$P_{\text{ave}} = \frac{1}{2} \omega \epsilon'' \int_v (\mathbf{E} \cdot \mathbf{E}^*)\, dv, \tag{4.5}$$

where $\epsilon''(T) = \sigma(T)/\omega$ and $\mathbf{H}^*$ and $\mathbf{E}^*$ are the complex conjugates of the magnetic and electric fields, respectively.

We assume that the heating occurs on a length scale much greater than a microwave length so that the heating may be averaged over a wavelength. This gives the source term

$$Q(T) = \frac{1}{2} \omega \epsilon'' |E|^2. \tag{4.6}$$

A complete analysis of this problem requires the solution of the double-diffusivity heat transfer model (2.12) with the source term (4.6) and of Maxwell's equations (4.1). These are coupled together via the temperature dependent dielectric loss term.

We decouple the equations by assuming the form of the electric field amplitude $|E|$. For constant material properties, the electric field amplitude in a semi-infinite domain has the form

$$|E| = E_o e^{-x\alpha/2}, \tag{4.7}$$

where E_o is the amplitude of the incident radiation and α is a decay constant.

The radiation decays exponentially with distance inside the grain bulk. We also assume this form to be physically reasonable for temperature dependent properties. Hence,

$$Q(T) = \frac{1}{2}\omega\epsilon'' E_o^2 e^{-\alpha x}. \tag{4.8}$$

Hill and Jennings [28] present the following forms of α:

$$\begin{aligned} \alpha &\approx \left(\frac{\omega\sigma}{2}\right)^{1/2} = \omega\left(\frac{e''}{2}\right)^{1/2}, \quad \text{for } \sigma/\omega = e'' \gg e', \\ \alpha &\approx \frac{\sigma}{2\sqrt{e'}} = \frac{\omega e''}{2\sqrt{e'}}, \quad \text{for } e'' \ll e'. \end{aligned} \tag{4.9}$$

To identify the body heating term $Q(T)$ as accurately as possible for a range of materials exposed to various microwave frequencies, Hill and Jennings [28] conducted an exhaustive survey of existing experimental results given by Von Hippel [31]. They show that for higher frequencies, which are the most useful frequencies in the consideration of microwave heating processes, the experimental data is very accurately approximated by both parabolic and linear fits for the body heating term $Q(T)$. For lower frequencies, one of two types of exponential curves provides an adequate fit to the experimental data. At intermediate frequencies, the experimental data exhibit both parabolic and exponential behaviour, so that a body heating term consisting of a linear combination of the two curves provides an adequate fit.

We will consider a cubic form for the body heating source term in our model, as this form applies directly to the microwave heating of grain. The cubic profile was determined by fitting a curve of best fit to results governing loss tangent versus temperature for shelled yellow-dent field corn, as determined in Trabelsi et al. [64].

4.2.2 Derivation of The Double-Diffusivity Heat Transfer Model Incorporating Microwave Heating

The one-dimensional double-diffusivity heat transfer model incorporating a body heating source term to account for heating due to microwave radiation, takes the form

$$\begin{aligned} \frac{\partial T_a(x,t)}{\partial t} &= K_a \frac{\partial^2 T_a(x,t)}{\partial x^2} - k_1 T_a(x,t) + k_1 T_g(x,t), \\ \frac{\partial T_g(x,t)}{\partial t} &= K_g \frac{\partial^2 T_g(x,t)}{\partial x^2} + k_2 T_a(x,t) - k_2 T_g(x,t) + \frac{Q_g(T_g(x,t))}{\rho_g c_g}, \end{aligned} \tag{4.10}$$

where T_a is the temperature of the air, T_g is the temperature of the grain, K_a is the thermal diffusivity of the air, K_g is the thermal diffusivity of the grain, ρ_g is the density of the grain, c_g is the specific heat of the grain at constant pressure and Q_g is the body heating source term due to microwave radiation.

The scenario which we consider is the same as that for the double-diffusivity heat transfer model. Furthermore, the grain is now considered to be heated via microwave radiation and the surrounding air via conduction from the boundary temperature and the surrounding grain, as illustrated in Figure 4.1. The heat transfer within the peripheral layer is most critical when internal convection cells are not fully established. Convective currents are thus assumed to be negligible, in order to allow analysis of such situations.

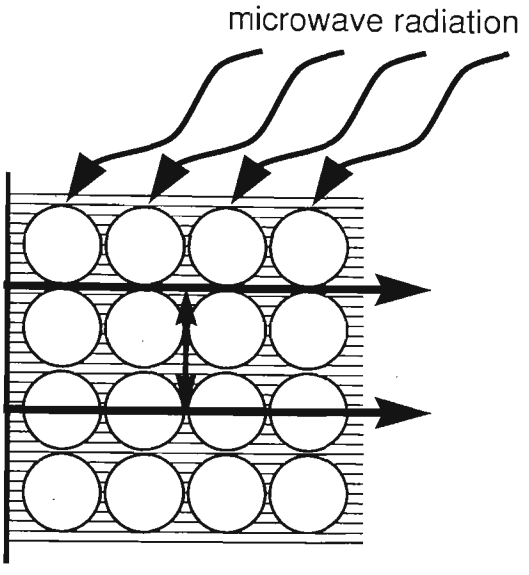

Figure 4.1: Idealisation of the double-diffusivity heat transfer model incorporating microwave heating.

4.3 A Semi-Analytical Approximation via the HBIM

In this section we illustrate the derivation of a semi-analytical approximation to the double-diffusivity heat transfer model incorporating microwave heating using the HBIM.

In Chapter 2 it was illustrated how the expression for the temperature T_a and the governing equation for the penetration depth through the air X_a were derived for the double-diffusivity heat transfer model. The expressions for the temperature T_a and the governing equation for the penetration depth through the air X_a for the double-diffusivity heat transfer model incorporating microwave heating are identical to those of the double-diffusivity heat transfer model, hence we will not re-derive them here. Instead, we will illustrate the derivation of the expressions for the temperature T_g and the governing equation for the penetration depth through the grain X_g, which differ to those of the double-diffusivity heat transfer model in that we now consider

a non-linear source term Q_g.

We will first determine an expression for T_g. We assume that there exists a penetration depth $x = X_g(t)$ beyond which there is effectively no heat flow. Thus, at $x = X_g$, we have

$$\begin{aligned} T_g &= T_{g0}, \\ \frac{\partial T_g}{\partial x} &= 0, \end{aligned} \tag{4.11}$$

since both temperature and heat flux must be continuous. Note that T_{g0} is the initial temperature of the grain, and as such is the internal temperature of the grain at the penetration point $x = X_g$.

Now, let us consider T_g at $x = X_g$. Upon differentiating both sides of equation $(4.11)_1$ with respect to time, we find

$$X_g' \frac{\partial T_g}{\partial x} + \frac{\partial T_g}{\partial t} = 0. \tag{4.12}$$

Hence, from equation $(4.11)_2$, we obtain

$$\frac{\partial T_g}{\partial t}(X_g, t) = 0. \tag{4.13}$$

Thus, at $x = X_g$, equation $(4.10)_2$ becomes

$$0 = K_g \frac{\partial^2 T_g}{\partial x^2} - k_2 T_g + k_2 T_a + \frac{Q_g(T_g)}{\rho_g c_g}, \tag{4.14}$$

and so, from equation $(4.11)_1$ we obtain

$$\frac{\partial^2 T_g}{\partial x^2}(X_g, t) = \frac{k_2}{K_g} T_{g0} - \frac{k_2}{K_g} T_a(X_g, t) - \frac{Q_g(T_{g0})}{K_g \rho_g c_g}, \tag{4.15}$$

which is a derived constraint. Hence, we have four conditions on T_g:

$$\begin{aligned} &T_g(0,t) = T_b(t), \qquad T_g(X_g,t) = T_{g0}, \\ &\frac{\partial T_g}{\partial x}(X_g,t) = 0, \qquad \frac{\partial^2 T_g}{\partial x^2}(X_g,t) = \frac{k_2}{K_g}T_{g0} - \frac{k_2}{K_g}T_a(X_g,t) - \frac{Q_g(T_{g0})}{K_g\rho_g c_g}, \end{aligned} \tag{4.16}$$

where $T_b(t)$ is the boundary temperature.

We now assume a cubic temperature profile for T_g in the spatial variable, with time-dependent coefficients:

$$T_g(x,t) = a(t) + b(t)x + c(t)x^2 + d(t)x^3, \tag{4.17}$$

and determine the values of the time-dependent coefficients using equations (4.16). We choose a cubic so there are four free parameters to match our four boundary conditions, one each for T_a and T_g at $x = 0$ and $x = \infty$.

Using (4.16), we obtain the following expressions for the four time-dependent coefficients

$$\begin{aligned} a &= T_b, \\ b &= \frac{3}{X_g}T_{g0} - \frac{3}{X_g}T_b + \frac{k_2 X_g}{2K_g}T_{g0} - \frac{k_2 X_g}{2K_g}T_a(X_g,t) - \frac{X_g}{2K_g\rho_g c_g}Q_g(T_{g0}), \\ c &= -\frac{3}{X_g^2}T_{g0} + \frac{3}{X_g^2}T_b - \frac{k_2}{K_g}T_{g0} + \frac{k_2}{K_g}T_a(X_g,t) + \frac{1}{K_g\rho_g c_g}Q_g(T_{g0}), \\ d &= \frac{T_{g0}}{X_g^3} - \frac{T_b}{X_g^3} + \frac{k_2}{2K_g X_g}T_{g0} - \frac{k_2}{2K_g X_g}T_a(X_g,t) - \frac{1}{2K_g X_g\rho_g c_g}Q_g(T_{g0}). \end{aligned} \tag{4.18}$$

Hence, upon substituting (4.18) into equation (4.17), the expression for T_g, becomes

$$\begin{aligned} T_g(x,t) &= T_{g0} + (T_b - T_{g0})\left(1 - \frac{x}{X_g}\right)^3 \\ &\left(k_2 T_{g0} - k_2 T_a(X_g,t) - \frac{Q_g(T_{g0})}{\rho_g c_g}\right)\left(\frac{X_g x}{2K_g} - \frac{x^2}{K_g} + \frac{x^3}{2K_g X_g}\right). \end{aligned} \tag{4.19}$$

Initially ($t = 0$), from equation $(4.10)_2$ we have

$$k_2 T_{g0} - k_2 T_{a0} = \frac{Q_g(T_{g0})}{\rho_g c_g}, \tag{4.20}$$

and by letting $T_{a0} = T_{g0} = T_0$, we obtain

$$\frac{Q_g(T_0)}{\rho_g c_g} = 0, \tag{4.21}$$

and hence, the expression for T_g becomes:

$$\begin{aligned} T_g(x,t) &= T_0 + (T_b - T_0)\left(1 - \frac{x}{X_g}\right)^3 \\ &- \frac{k_2 X_g x}{2K_g}(T_a(X_g,t) - T_0)\left(1 - \frac{x}{X_g}\right)^2. \end{aligned} \tag{4.22}$$

In Chapter 2 we obtained an expression for T_a, equation (2.28), by assuming a penetration depth $x = X_a(t)$, using an analogous procedure.

Once we determine an expressions for X_g, an explicit expression for T_g will exist, given by equation (4.22).

We now let

$$\Phi_g(t) = \int_0^{X_g} T_g \, dx, \tag{4.23}$$

so that equation $(4.10)_2$ will be satisfied in an averaged or integral sense over the interval $[0, X_g]$. Upon differentiating both sides with respect to time, we have

$$\frac{d\Phi_g}{dt} = \int_0^{X_g} \frac{\partial T_g}{\partial t} \, dx + T_g(X_g,t) X_g'. \tag{4.24}$$

Thus, from equations $(4.10)_2$, $(4.11)_1$ and $(4.11)_2$, we obtain the following expression which becomes the governing expression for X_g:

$$\frac{d\Phi_g}{dt} = -K_g\frac{\partial T_g}{\partial x}(0,t) - k_2\Phi_g + k_2\int_0^{X_g} T_a\,dx + T_0X_g' + \frac{1}{\rho_g c_g}\int_0^{X_g} Q_g(T_g)\,dx. \tag{4.25}$$

We must now determine expressions for

$$\Phi_g,\ \frac{\partial T_g}{\partial x}(0,t),\ \int_0^{X_g} Q_g(T_g)\,dx \text{ and } \int_0^{X_g} T_a\,dx. \tag{4.26}$$

Upon differentiating equation (4.22) with respect to x, we obtain

$$\frac{\partial T_g}{\partial x}(0,t) = -\frac{3}{X_g}(T_b - T_0) - \frac{k_2X_g}{2K_g}(T_a(X_g,t) - T_0). \tag{4.27}$$

By using the expression for T_g, that is, equation (4.22), equation (4.23) becomes

$$\Phi_g = T_0X_g + \frac{X_g}{4}(T_b - T_0) - \frac{X_g^3k_2}{24K_g}(T_a(X_g,t) - T_0). \tag{4.28}$$

Finally, from equation (2.28), we obtain

$$\begin{aligned}\int_0^{X_g} T_a\,dx &= T_bX_g + \frac{X_g^2}{X_a}(T_b - T_0)\left(-\frac{3}{2} + \frac{X_g}{X_a} - \frac{X_g^2}{4X_a^2}\right)\\ &- \frac{k_1X_aX_g^2}{2K_a}(T_g(X_a,t) - T_0)\left(\frac{1}{2} - \frac{2X_g}{3X_a} + \frac{X_g^2}{4X_a^2}\right).\end{aligned} \tag{4.29}$$

It follows then, from using the fact that at $x = X_g$

$$\frac{d}{dt}T_a(X_g,t) = \frac{\partial T_a}{\partial x}(X_g,t)X_g' + \frac{\partial T_a}{\partial t}(X_g,t), \tag{4.30}$$

that the governing equation for X_g, equation (4.25), becomes

$$T_b'X_g + X_g'(T_b - T_0) - \frac{\partial T_a}{\partial x}(X_g,t)\frac{X_g'X_g^3k_2}{6K_g}$$

$$
\begin{aligned}
- & \frac{\partial T_a}{\partial t}(X_g,t)\frac{k_2 X_g^3}{6K_g} - (T_a(X_g,t)-T_0)\frac{k_2 X_g^2 X_g'}{2K_g} \\
= & (T_b - T_0)\left(\frac{12K_g}{X_g} - k_2 X_g\right) \\
+ & (T_b - T_0)\frac{4k_2 X_g^2}{X_a}\left(-\frac{3}{2} + \frac{X_g}{X_a} - \frac{X_g^2}{4X_a^2}\right) \\
+ & (T_a(X_g,t) - T_0)2k_2 X_g\left(1 + \frac{k_2 X_g^2}{12K_g}\right) \\
+ & (T_g(X_a,t) - T_0)\frac{4k_1 k_2 X_g^2}{K_a}\left(\frac{X_g}{3} - \frac{X_a}{4} - \frac{X_g^2}{8X_a}\right) \\
- & 4X_g\left(k_2 T_b - k_2 T_0\right) + \frac{4}{\rho_g c_g}\int_0^{X_g} Q_g(T_g)\,dx.
\end{aligned}
\tag{4.31}
$$

Similarly, the governing equation for X_a, equation (2.39), was derived in Chapter 2.

In the next section we derive the form of the governing equation for X_g, using a cubic body heating source term. This cubic profile was determined by fitting a curve of best fit to the results governing loss tangent versus temperature for shelled yellow-dent field corn, as determined in Trabelsi et al. [64].

4.3.1 A Cubic Body Heating Source Term

Trabelsi et al. [64] conducted a study of the dielectric properties of shelled, yellow-dent field corn, measured at different bulk densities and moisture contents. Grain temperatures ranged from 4°C to 45°C, grain moisture contents ranged from 9%

to 19% wet basis and the frequencies ranged from 11GHz to 18GHz. Of particular interest to us are their results that pertain to the loss factor versus temperature of corn at 14.5% moisture content. Shelled, yellow-dent corn at such a moisture content represents properties typical of most grains of interest to the Australian grain industry, and hence was chosen to use here. A curve of best fit was fitted to this data and a cubic profile of the following form was obtained for the loss factor

$$\epsilon''(T) = A' + B'T + C'T^2 + D'T^3, \tag{4.32}$$

where A', B', C' and D' are constants.

By assuming the following form for the body heating source term

$$Q_g(T_g) = \left(A + B\,T_g + C\,T_g^2 + D\,T_g^3\right) e^{-\alpha x}, \tag{4.33}$$

where

$$A = A'L, \quad B = B'L, \quad C = C'L, \quad D = D'L \quad \text{and} \quad L = \frac{\omega E_o^2}{2}, \tag{4.34}$$

and E_o is the incident electric field amplitude, we obtain

$$\int_0^{X_g} Q_g(T_g)dx \;=\; F\left(A, B, C, D, T_0, T_b, X_a, X_g, \alpha, k_1, k_2, K_a, K_g\right). \tag{4.35}$$

We derive the general form F of the integral only. This calculation was computed by Maple and is very lengthy, and as such is not presented here.

Hence, the governing equation for X_g, equation (4.31), becomes

$$T_b'X_g + X_g'(T_b - T_0) - \frac{\partial T_a}{\partial x}(X_g, t)\frac{X_g' X_g^3 k_2}{6K_g}$$

$$
\begin{aligned}
- & \frac{\partial T_a}{\partial t}(X_g,t)\frac{k_2 X_g^3}{6K_g} - (T_a(X_g,t)-T_0)\frac{k_2 X_g^2 X_g'}{2K_g} \\
= & (T_b - T_0)\left(\frac{12K_g}{X_g} - k_2 X_g\right) \\
+ & (T_b - T_0)\frac{4k_2 X_g^2}{X_a}\left(-\frac{3}{2} + \frac{X_g}{X_a} - \frac{X_g^2}{4X_a^2}\right) \\
+ & (T_a(X_g,t) - T_0)2k_2 X_g\left(1 + \frac{k_2 X_g^2}{12K_g}\right) \\
+ & (T_g(X_a,t) - T_0)\frac{4k_1 k_2 X_g^2}{K_a}\left(\frac{X_g}{3} - \frac{X_a}{4} - \frac{X_g^2}{8X_a}\right) \\
- & 4X_g\left(k_2 T_b - k_2 T_0\right) \\
+ & \frac{4}{\rho_g c_g} F\left(A,B,C,D,T_0,T_b,X_a,X_g,\alpha,k_1,k_2,K_a,K_g\right).
\end{aligned}
\tag{4.36}
$$

In order to obtain expressions for $X_a(t)$ and $X_g(t)$, the coupled system of equations (2.39) and (4.36), must be solved. This needs to be done numerically due to the complexity of the expressions.

4.4 Some Results

In this section we discuss results pertaining to the semi-analytical approximation of the double-diffusivity heat transfer model incorporating microwave heating as

developed using the HBIM. We compare these solutions to numerical approximations obtained by the explicit FTCS finite-difference scheme. We also compare these results to the case involving no microwave heating source, that is, the simplified double-diffusivity heat transfer model as developed in Chapter 2.

The coupled system of equations for $X_a(t)$ and $X_g(t)$, equations (2.41) and (4.36), was solved numerically using the Fehlberg fourth-order Runge-Kutta method as implemented in MAPLE. The value of α was calculated from equation (4.9).

The same parameter values are used as those in Chapter 2, along with the following microwave heating specific values [46, 64]: $\omega = 1000\,\text{Hz}$, $E_o^2 = 40\,\text{Vm}^{-1}$, $A' = 0.2863$, $B' = 0.0243$, $C' = -9.5792E-04$, $D' = 1.36E-05$ and $\alpha = 250\ \text{m}^{-1}$. The scenario we envisage is that of a silo wall heated by an ambient temperature of $10\,^{\circ}\text{C}$ with the air and grain at an initial temperature of $0\,^{\circ}\text{C}$. This is typical of conditions when grain is harvested and stored in cool climates. Furthermore, we consider the grain bulk to be heated by a microwave source, as is the case with heat disinfestation via microwave radiation. As this is currently an expensive form of disinfestation, it is presently envisaged to be only used for niche applications, such as for the fast disinfestation of a small batch of grain prior to export.

Figure 4.2 shows the variation of the penetrations depths $X_a(t)$ and $X_g(t)$ with time, up to $t = 1000$ seconds. Shown are the semi-analytical approximations to the double-diffusivity heat transfer model incorporating microwave heating, equations (2.41) and (4.36). We observe that there exists a noticeable difference in the profiles of the two penetration fronts. As a result of the grain being heated directly by microwave radiation, the penetration front through the grain continues to in-

crease, as opposed to the eventual levelling-off of the penetration front through the air. This results in the penetration front through the grain eventually becoming greater than the penetration front through the air. This does not occur until approximately $t = 850$ seconds has elapsed. An increase in microwave power simply results in this occuring earlier.

Figure 4.3 shows the variation of the temperatures T_a and T_g with distance, up to $t = 20$ seconds. Shown is the semi-analytical approximation, equations (2.28) and (4.22), and the numerical approximation to the double-diffusivity heat transfer model incorporating microwave heating (4.10). At an early time and with relatively low microwave power, there is an observed difference in the evolution of the air and grain temperature profiles. An increase in power, or time, results in this difference

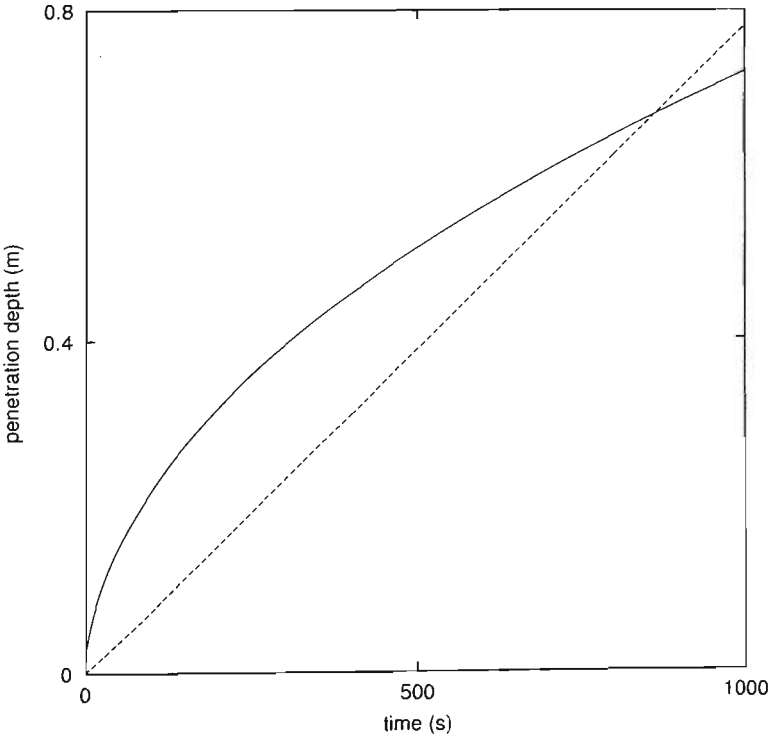

Figure 4.2: Semi-analytical approximations of the penetration depths X_a (—) and X_g (– –) versus time, up to $t = 1000$ seconds, for the double-diffusivity heat transfer model incorporating microwave heating.

decreasing, and eventually, the temperature of the grain becomes greater than the temperature of the air, as the grain absorbs the microwave radiation. If the power is kept at the current level, this will occur after approximately $t = 850$ seconds, as seen in Figure 4.2. The agreement between the semi-analytical and numerical solutions is found to be very good.

We now compare our results for the double-diffusivity heat transfer model incorporating microwave heating to a case involving no microwave heating source, that is, the simplified double-diffusivity heat transfer model as developed in Chapter 2. We do this to illustrate the effect which microwave radiation has upon the predicted air and grain temperatures.

Figure 4.4 shows the variation of both the penetration depths $X_a(t)$ and $X_g(t)$

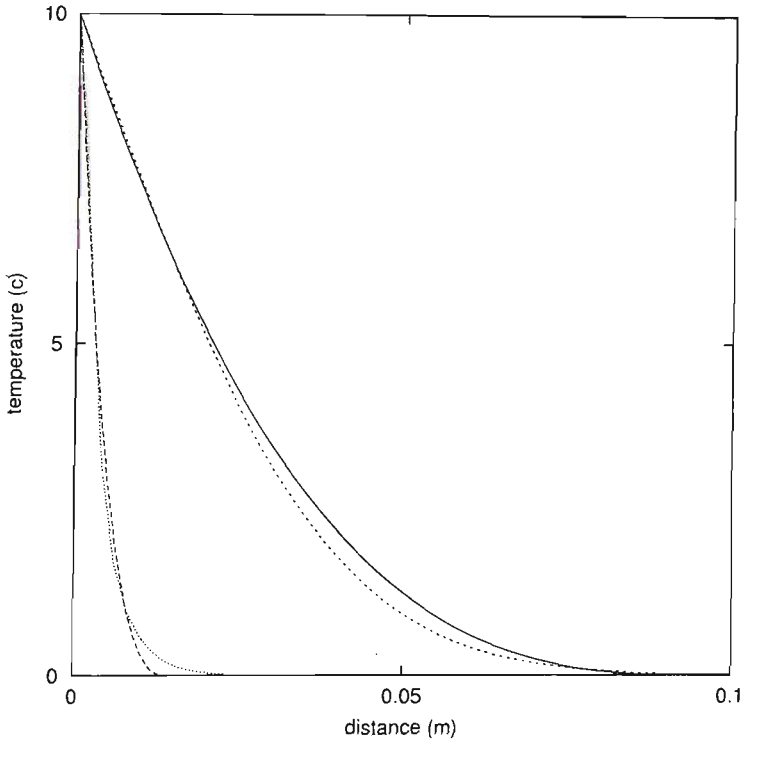

Figure 4.3: Semi-analytical and numerical approximations of the temperatures T_a, (—) and (- -), and T_g, (– –) and $(\cdots)$, versus distance, up to $t = 20$ seconds, for the double-diffusivity heat transfer model incorporating microwave heating.

with time, up to $t = 1000$ seconds. Shown are the semi-analytical approximations to the double-diffusivity heat transfer model incorporating microwave heating, equations (2.28) and (4.22), and the double-diffusivity heat transfer model, equations (2.54) and (2.55). We observe that the difference in grain temperature predictions of the two models is noticeably different, as expected. With the double-diffusivity heat transfer model incorporating microwave heating the grain is heated via microwave radiation, which results in the grain heating up much faster than the surrounding air as the grain is heated directly by microwave radiation whilst the air in the silo is heated by convection only, from the boundary and the hotter grains. The difference between the air temperature predictions of the two models is not as great, as the air is heated via convection, and the value of the coupling terms

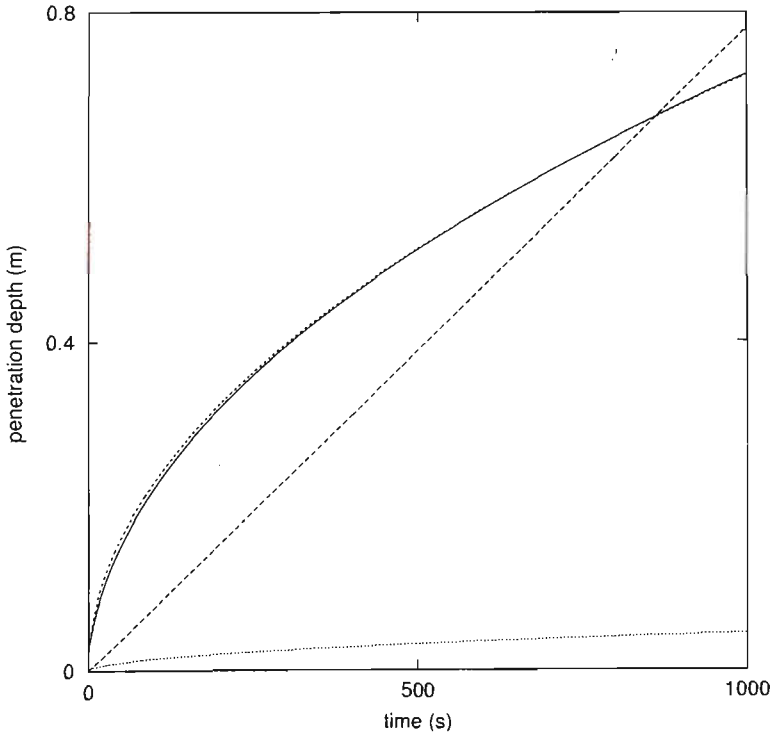

Figure 4.4: Double-diffusivity heat transfer model incorporating microwave heating and double-diffusivity heat transfer model approximations of the penetration depths X_a, (—) and (- -), and X_g, (– –) and $(\cdots)$, versus time, up to $t = 1000$ seconds.

between the air and grain, k_1 and k_2, which are based on the *effective* heat transfer coefficient k_a, are relatively low.

Figure 4.5 shows the variation of both the temperatures $T_a(t)$ and $T_g(t)$ with distance, up to $t = 20$ seconds. Shown are the semi-analytical approximations to the double-diffusivity heat transfer model incorporating microwave heating equations (2.28) and (4.22), and the double-diffusivity heat transfer model, equations (2.54) and (2.55). Once again, we observe that the grain temperature predictions of the two models differ noticeably, as expected, since grain that is heated via microwave radiation will heat up faster, resulting in it penetrating further into the grain bulk, as is observed. The difference between the air temperature predictions of the two models is once again seen to be near negligible.

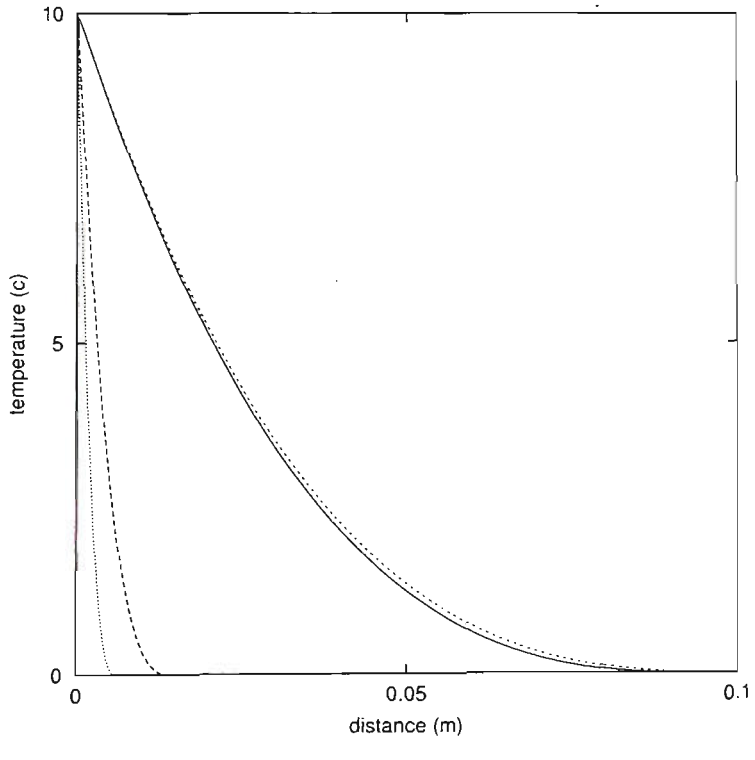

Figure 4.5: Double-diffusivity heat transfer model incorporating microwave heating and double-diffusivity heat transfer model approximations of the temperatures T_a, (—) and (- -), and T_g, (– –) and $(\cdots)$, versus distance, up to $t = 20$ seconds.

4.5 Conclusions

In this chapter we have outlined the derivation of the double-diffusivity heat transfer model incorporating microwave heating, by appending a non-linear body heating source term to the double-diffusivity heat transfer model which was developed in Chapter 2.

We have derived a semi-analytical approximation to the double-diffusivity heat transfer model incorporating microwave heating using the HBIM, and we have compared this approximation to one obtained numerically based on an explicit finite-difference scheme. We have shown by way of some results that the two approximations agree very well to one another. We have also compared this model to the double-diffusivity heat transfer model developed in Chapter 2, in order to illustrate the difference in air and grain temperature profiles of a grain bulk exposed to microwave radiation with one that is simply exposed to ambient air. The results agree with what is expected, that is, that microwave heating significantly affects the temperature of the grain, and to a lesser extent, the air as well. They also predict, as do the results of the double-diffusivity heat transfer and the two-stage heat transfer models, that there exists a noticeable difference between the air and grain temperatures of a grain bulk, which is most apparent for early time.

Chapter 5

Conclusions

An understanding of the flow of heat in grain stores, particularly within the peripheral layer, is important from many industrial perspectives, such as when dealing with insect infestation. In this thesis we have developed three mathematical models that allow us to examine such issues. These models provide better insight into the dynamics of the heat flow than the analysis that exists in the literature to date.

Two of the models, namely the doubly-diffusivity heat transfer model and the two-stage heat transfer model, allow predictions to be made of the variation in the air and grain temperatures within a grain bulk, primarily within the peripheral layer. Semi-analytical approximations obtained using the HBIM allow us to analyse some of the important factors involved with such processes, resulting in a better understanding. Both models predict that there exists a difference between the air and grain temperatures of a grain bulk, which is most apparent for early time.

The third model, the double-diffusivity heat transfer model incorporating microwave heating, allows us to predict the variation in the air and grain temperatures

of a grain bulk exposed to microwave radiation. By adapting an approach that involves modelling the microwave heating process by a body heating source term, we are able to make predictions from a semi-analytical viewpoint relatively easily, to once again, allow analysis of such processes.

These models are very important since previously, no work has been done in analysing the difference between the air and grain temperatures within the peripheral layer, either qualitatively or quantitatively. The proposed modelling of the heat flow, by either linear or relatively simple non-linear models, allows the formulation of semi-analytical approximations that provide important insight into the difference that exists between the air and grain temperatures of a grain bulk, in particular, for small time and spatial scales, within the peripheral layer. The approximations obtained for all three models are physically reasonable, but exact agreement will not be known until experimental data can be obtained. At present, there is no direct experimental data available, due to the difficulty involved in measuring air and grain temperatures separately, particularly, within the peripheral layer.

The three mathematical models developed in this thesis form the foundations for subsequent work to what are very complex practical problems, which we believe will ultimately lead to a better understanding of the microclimate within the peripheral layer of a grain bulk.

Bibliography

[1] Antic, A., and Hill, J. M.: 'A Mathematical Model for Heat Transfer in Grain Store Microclimates'. *Aust. N.Z. Ind. Appl. Math. J.* **42 (E)** (2000) C117-C133.

[2] Antic, A., and Hill, J. M.: 'A Two-Stage Heat Transfer Model for the Peripheral Layers of a Grain Store'. *J. Appl. Math. Dec. Sc.* **7** (2003) 147-164.

[3] Antic, A., and Hill, J. M.: 'The Double-Diffusivity Heat Transfer Model for Grain Stores incorporating Microwave Heating'. *J. Appl. Math. Mod.* **27** (2003) 629-647.

[4] Aifantis, E. C.: 'Continuum Basis for Diffusion in Regions with Multiple Diffusivity'. *J. Appl. Phys.* **50** (1979) 1334-1338.

[5] Aifantis, E. C.: 'Introducing a Multiporous Medium'. *Developments in Mechanics, Proc. 15th Midwestern Mech. Conf.* **8** (1977) 209-211.

[6] Aifantis, E. C.: 'A New Interpretation of Diffusion in High-Diffusivity Paths: A Continuum Approach'. *Acta. Metallurgica* **27** (1979) 683-691.

[7] Aifantis, E. C., and Hill, J. M.: 'On the Theory of Diffusion in Media with Double Diffusivity I: Basic Mathematical Results'. *Quart. J. Mech. Appl. Math.* **33** (1980) 1-21.

[8] Babcock, R. E., Green, D. W., and Perry, R. H.: 'Longitudinal Dispersion Mechanisms in Packed Beds'. *Amer. Inst. Chem. Eng. J.* **12** (1966) 922-927.

[9] Banks, H. J.: 'Prospects for Heat Disinfestation'. *Aust. Postharvest Tech. Conf., Canberra, 26-29 May* (1998) 227-232.

[10] Barenblatt, G. I., Zheltov, Iu. P., and Kochina, I. N.: 'Basic Concepts in the Theory of Seepage of Homogeneous Liquids in Fissured Rocks'. *J. Appl. Math. Mech.* **24** (1960) 1286-1303.

[11] Beckett, S.: 'Treating psocids with Heat: An Alternative Grain Disinfestation Treatment for a New Pest'. *Aust. Postharvest Tech. Conf., Canberra, 26-29 May* (1998) 334-337.

[12] Carslaw, H. S., and Jaeger, J. C.: *Conduction of Heat in Solids.* Clarendon Press, Oxford. (1965).

[13] Çengel, Y. A.: *Heat Transfer: A Practical Approach.* McGraw-Hill. (1998).

[14] Chen, X. D.: 'Self-Heating Behaviour of Low Moisture Content Particles - Modelling the basket-Heating of Solid Particles and Some Aspects of the Cross Over Behaviour Using Milk Powder as an Example'. *Aust. N.Z. Ind. Appl. Math. J.* **43** (2001) 165-181.

[15] Coleman, C. J.: 'The Microwave Heating of Frozen Substances'. *J. Appl. Math. Mod.* **14** (1990) 439-443.

[16] Coleman, C. J.: 'On the Microwave Hotspot Problem'. *J. Aust. Math. Soc. (Series B)* **33** (1991) 1-8.

[17] Collins, P. J.: 'Insect Pest Trends in the Farm System'. *Aust. Postharvest Tech. Conf., Canberra, 26-29 May* (1998) 43-45.

[18] Collins, P. J.: 'Resistance to Grain Protectants and Fumigants in Insect Pests of Stored Products in Australia'. *Aust. Postharvest Tech. Conf., Canberra, 26-29 May* (1998) 55-57.

[19] Darby, J.: 'Putting Grain Aeration in Order with Generalised Aeration Categories'. *Aust. Postharvest Tech. Conf., Canberra, 26-29 May* (1998) 203-208.

[20] Darby, J.: 'Storage Success Depends on Careful Selection'. *Farming Ahead No. 93* (1999) 53-54.

[21] Davis, G. B.: *Mathematical Modelling of Rate-Limiting Mechanisms of Pyritic Oxidation in Overburden Dumps*, PhD Thesis, University of Wollongong. (1983).

[22] Fohr, J-P., and Moussa, H. B.: 'Heat Conduction Mass Transfer in a Cylindrical Grain Silo Submitted to a Periodical Wall Heat Flux'. *Int. J. Heat Mass Trans.* **37** (1994) 1699-1712.

[23] Hill, J. M.: 'A Discrete Random Walk Model for Diffusion in Media with Double Diffusivity'. *J. Aust. Math. Soc. (Series B)* **22** (1980) 58-75.

[24] Hill, J. M.: 'On the Solution of Reaction-Diffusion Equations'. *IMA. J. Appl. Math.* **27** (1981) 177-194.

[25] Hill, J. M.: 'Some Theoretical Aspects of Diffusion in the Presence of High-Diffusivity Paths'. *Scripta Metallurgica* **13** (1979) 1027-1031.

[26] Hill, J. M., and Aifantis, E. C.: 'On the Theory of Diffusion in Media with Double Diffusivity II: Boundary-Value Problems'. *Quart. J. Mech. Appl. Math.* **33** (1980) 23-41.

[27] Hill, J. M., and Dewynne, J. N.: *Heat Conduction.* Blackwell Scientific Publications, Boston. (1987).

[28] Hill, J. M., and Jennings, M. J.: 'Formulation of model equations for heating by microwave radiation'. *J. Appl. Math. Mod.* **17** (1993) 369-379.

[29] Hill, J. M., and Pincombe, A. H.: 'Some Similarity Temperature Profiles for the Microwave Heating of a Half-Space'. *J. Aust. Math. Soc. (Series B)* **33** (1992) 290-320.

[30] Hill, J. M., and Smyth, N. F." 'On the Mathematical Analysis of Hot-Spots Arising from Microwave Heating'. *Math. Engng. Ind.* **2** (1990) 267-278.

[31] Hippel, A. R. Von.: *Dielectrical Materials and Applications*, MIT Press, Cambridge, MA. (1954).

[32] Jia, C., Sun, D-W., and Cao, C.: 'Finite Element Prediction of Transient Temperature Distribution in a Grain Storage Bin'. *J. Agric. Engng. Res.* **76** (2000) 323-330.

[33] Jia, C., Sun, D-W., and Cao, C.: 'Mathematical Simulation of Temperature and Moisture Fields within a Grain Kernel During Drying'. *Drying Technology* **18** (2000) 1305-1325.

[34] Jolly, P., and Turner, I.: 'Nonlinear Field Solutions of One-Dimensional Microwave Heating'. *J. Micr. Power* **25** (1990) 3-15.

[35] Kreigsmann, G. A., Brodwin, M. E., and Walters, D. G.: 'Microwave Heating of a Ceramic Halfspace'. *Soc. Ind. Appl. Math. J. Appl. Math.* **50** (1990) 1088-1098.

[36] Landahl, H. D.: *Bull. Math. Biophys.* **15** (1953) 49.

[37] Ma, Y. H., and Lee, T. Y.: *Amer. Inst. Chem. Eng. J.* **22** (1976) 147.

[38] Massoudi, M., and Phuoc, T. X.: 'Flow and Heat Transfer Due to Natural Convection in Granular Methods'. *Int. J. Non-Lin. Mech.* **34** (1999) 347-359.

[39] McGuinness, M. J.: 'Pressure Transmission in a Bounded Randomly Fractured Reservoir of Single-Phase Fluid'. *Trans. in Por. Med.* **1** (1986) 371-397.

[40] McNabb, A.: 'Factorizable 'Fruit Cake' Boundary Value Problems'. *Suppl. Newsletter No. 12 N.Z. Math. Soc.* (1978) 9-18.

[41] Metaxas, A. C., and Meredith, R. J.: *Ind. Micr. Heating*, Peter Peregrinus Ltd, London, UK. (1988).

[42] Moench, A. F.: 'Double-Porosity Models for a Fissured Groundwater Reservoir with Fracture Skin'. *Water Resources. Res.* **20** (1984) 831-846.

[43] Molz, F. J.: *J. Theor. Biol.* **59** (1976) 277.

[44] Mor, L., Mor, L. A., Sideman, S., and Brandes, J. M.: *Chem. Engng. Sci.* **34** (1980) 725.

[45] Nelson, S. O.: 'Review and Assessment of Radio-Frequency and Microwave Energy for Stored-Grain Insect Control'. *Trans. Amer. Soc. Agr. Eng.* **39** (1996) 1475-1484.

[46] Nelson, S. O., Bartley, P. G., and Lawrence, K. C.: 'RF and Microwave Dielectric Properties of Stored-Grain Insects and their Applications for Potential Insect Control'. *Trans. Amer. Soc. Agr. Eng.* **41** (1998) 685-692.

[47] Parry, J. L.: 'Mathematical Modelling and Computer Simulation of Heat and Mass Transfer in Agricultural Grain Drying: A Review'. (1964).

[48] Pohlhausen, K.: *Z. Angew. Math. Mech.* **1** (1921) 252.

[49] Portis, A. M.: *Electromagnetic Fields: Sources and Media*, John Wiley and Sons, New York, US. (1978).

[50] Prabhu, N. U.: *Stochastic Processes*, Macmillan. (1966).

[51] Pruess, K.: 'A Practical Method for Modelling Fluid and Heat Flow in Fractures Porous Media'. *Soc. Pet. Eng. J.* (1985) 14-26.

[52] Rees, D.: 'Psocids as Pests of Australian Grain Stores'. *Aust. Postharvest Tech. Conf., Canberra, 26-29 May* (1998) 46-51.

[53] Rees, D.: 'Countering the Growing Threat of psocids to Australian Grain'. *Stored Grain Australia Newsletter* (1999).

[54] Rubinstein, L. I.: 'Process of Conduction of Heat in Heterogeneous Media'. *Izv. Akad. Nauk. SSSR, Geogr.* **12** (1948) 12-45.

[55] Skopp, J., and Warrick, A. W.: 'A Two-Phase Model for the Miscible Displacement of Reactive Solutions in Soils'. *Proc. Soil Sc. Soc. Am.* **38** (1974) 545-550.

[56] Smyth, N. F.: 'Microwave Heating of Bodies with Temperature Dependent Properties'. *Wave Motion* **12** (1990) 171-186.

[57] Snelson, J. T.: 'Use of Insecticides: General Principles'. *Proceedings of the Australian Development Assistance Course on the Preservation of Stored Cereals: Volume 2.* CSIRO Division of Entomology. (1984) 589-604.

[58] Stehfest, H.: 'Algorithm 368: Numerical Inversion of Laplace Transform'. *Comm. Assoc. Comp. Mach.* **13** (1970) 47-49.

[59] Streltsova-Adams, T. D.: *Adv. Hydrosci.* **11** (1979) 357.

[60] Sullivan, W. N., and Sabersky, R. H.: 'Heat Transfer to Flowing Granular Media'. *Int. J. Heat Mass Transfer* **18** (1975) 97-107.

[61] Sutherland, J. W., Banks, P. J., and Griffiths, H. J.: 'Equilibrium Heat and Moisture Transfer in Air Flow Through Grain'. *J. Agr. Engng. Res.* **16** (1971) 368-386.

[62] Thorpe, G. R., and Whitaker, S.: 'Local Mass and Thermal Equilibria in Ventilated Grain Bulks Part I: The Development of Heat and Mass Conservation Equations'. *J. Stored Prod. Res.* **28** (1992) 15-27.

[63] Thorpe, G. R., and Whitaker, S.: 'Local Mass and Thermal Equilibria in Ventilated Grain Bulks Part II: The Development of Constraints'. *J. Stored Prod. Res.* **28** (1992) 29-54.

[64] Trabelsi, S., Kraszewski, A. W., and Nelson, S. O.: 'Microwave Dielectric Properties of Shelled, Yellow-Dent Field Corn'. *J. Micr. Power & Electromagnetic Energy* **32** (1997) 188-194.

[65] Turner, G. A.: *Chem. Engng. Sci.* **7** (1958) 156.

[66] Vargas, W. L., and McCarthy, J. J.: 'Unsteady Heat Conduction in Granular Materials'. *Mat. Res. Soc. Symp. Proc.* **627** (2000) BB3.9.1-BB3.9.6.

[67] Vortmeyer, D., and Schaefer, R. J.: 'Equivalence of One- and Two-Phase Models for Heat Transfer Processes in Packed Beds: One Dimensional Theory'. *Chem. Eng. Sci.* **29** (1973) 485-491.

[68] Warren, J. E., and Root, P. J.: 'The Behaviour of Naturally Fractured Reservoirs'. *Soc. Pet. Eng. J.* (1963) 245-255.

List of Publications of the Author

1. Antic, A., and Hill, J. M.: 'A Mathematical Model for Heat Transfer in Grain Store Microclimates'. *Aust. N.Z. Ind. Appl. Math. J.* **42 (E)** (2000) C117-C133.

2. Antic, A., and Hill, J. M.: 'A Two-Stage Heat Transfer Model for the Peripheral Layers of a Grain Store'. *J. Appl. Math. Dec. Sc.* **7** (2003) 147-164.

3. Antic, A., and Hill, J. M.: 'The Double-Diffusivity Heat Transfer Model for Grain Stores incorporating Microwave Heating'. *J. Appl. Math. Mod.* **27** (2003) 629-647.